Norway grants

Ammonia as carbon free fuel for internal CombusTion engIne driVen AgriculTural vEhicle

ACTIVATE

Work Package 5
Deliverable Report

Topic: D5.4

Final report for activities in WP5. Final report will consist detail description of carried out test, collected data, analysis as well as description of all founding for developed ACTIVATEngine technology.

Programme operated by: NCBR National Centre for Research and Development

Project consortium: Silesian University of Technology, NTNU Norwegian University of Science and Technology, LOGE, University of Agriculture in Krakow

Norway grants

Contents

1 Tractor and engine tests

1.1 Data set Generation for agriculture tractor testing

The set of data collected at developed in the frame of the ACTIVATE project test-rig, equipped with 4-stork Lifan Diesel C186 engine (see Tab. 1) was collected for constant RPM 1500. Test was performed using two configuration of the ammonia injectors in order to check influence of spatial configuration of the injector on engine operation. Test configuration presented in table 2 was performed for different Ammonia Energy Share (AES) where amount of biodiesel was kept constant while ammonia flow rate was changed. For biodiesel and ammonia constant injection timing before top death center piston position was set, 16 and 14 CAD, respectively. The analyzed parameters by application of the developed computational procedure, calculated based on the indicated pressure profile were

- IMEP - Indicated Mean Effective Pressure,
- HRR - Heat Release Rate - during combustion stage,
- pressure,
- emission of selected species.

Figure 1 presents indicated pressure profile for investigated cases in Test 1. It can be noticed marginal differences between subsequent profiles which also can be seen in figure 2. The idea of performed test was to keep the same Indicated Mean Effective Pressure and generated power which was successfully achieved for different ammonia energy shares. IMEPs for cindered engine operational condition are presented din figure 3. Preformed test also shows small variation in HRR between tested AESs, see Fig. 4. The fluctuation of calculated ln(p) for 6 cases is illustrated in figure 5.

Table 1: Specifications of diesel engine: IVO - Inlet Valve Opening; IVC - Inlet Valve Closing; EVO - Exhaust Valve Opening; EVC - Inlet Valve Closing; SOI - Start of Injection

Engine info.	Valves	Units
Engine model	4 stroke, Lifan	
Bore and stroke	86×70	mm
Geometric CR	16.5:1	
Maximum power (3500 rpm)	6.4	kW
Conn. rod length	117.5	mm
IVO	14°	BTDC
IVC	45°	ABDC
EVO	50°	BBDC
EVC	16°	ATDC
SOI	-15.5	BTDC
Injection pressure	200	bar

Table 2: Test 1 - engine operational parameters

Name	m_{bio}, kg/h	m_{NH_3},, kg/h	N, kW	IMEP, bar	AES
A	0.491	0.709	1.763	5.73	0.42
B	0.488	0.829	1.744	5.73	0.46
C	0.481	0.993	1.794	5.80	0.51
D	0.473	1.084	1.768	5.79	0.53
E	0.466	1.248	1.732	5.71	0.57
F	0.454	1.466	1.641	5.43	0.62

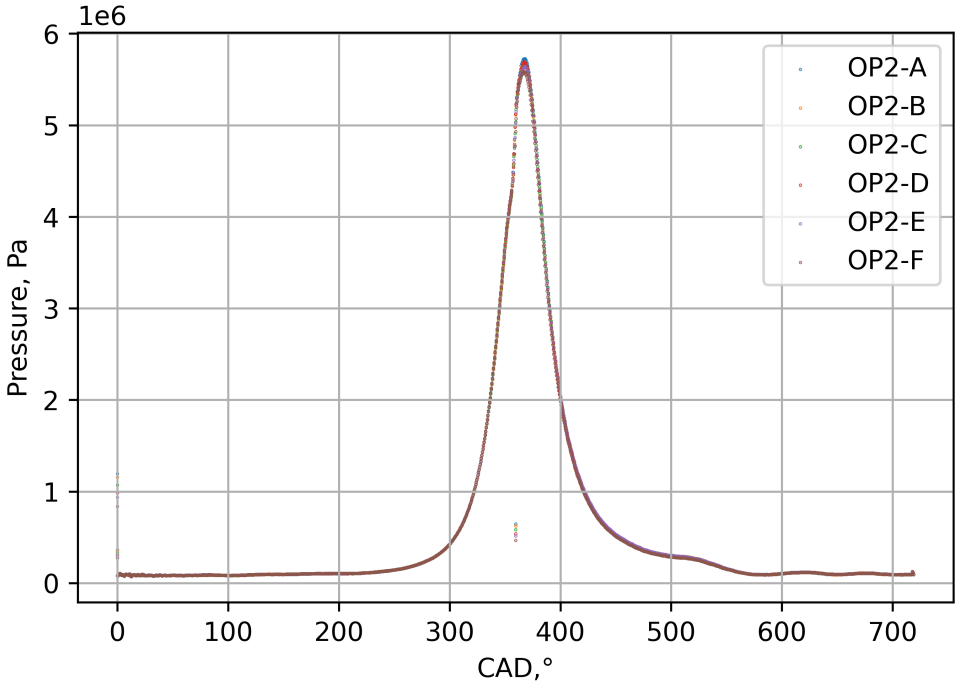

Figure 1: Pressure profiles for test 1

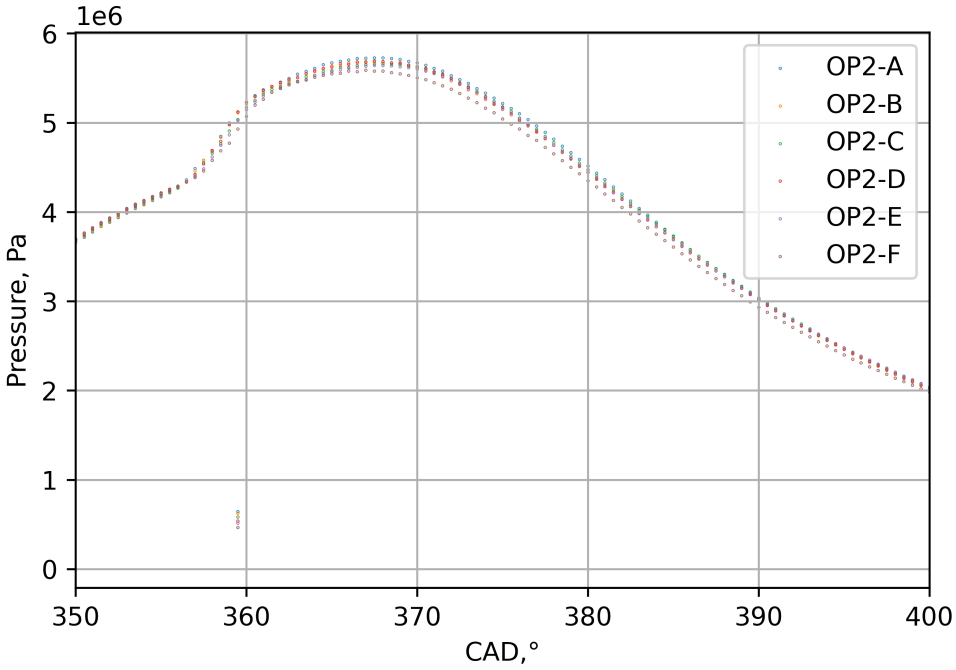

Figure 2: Clipped pressure profiles for test 1

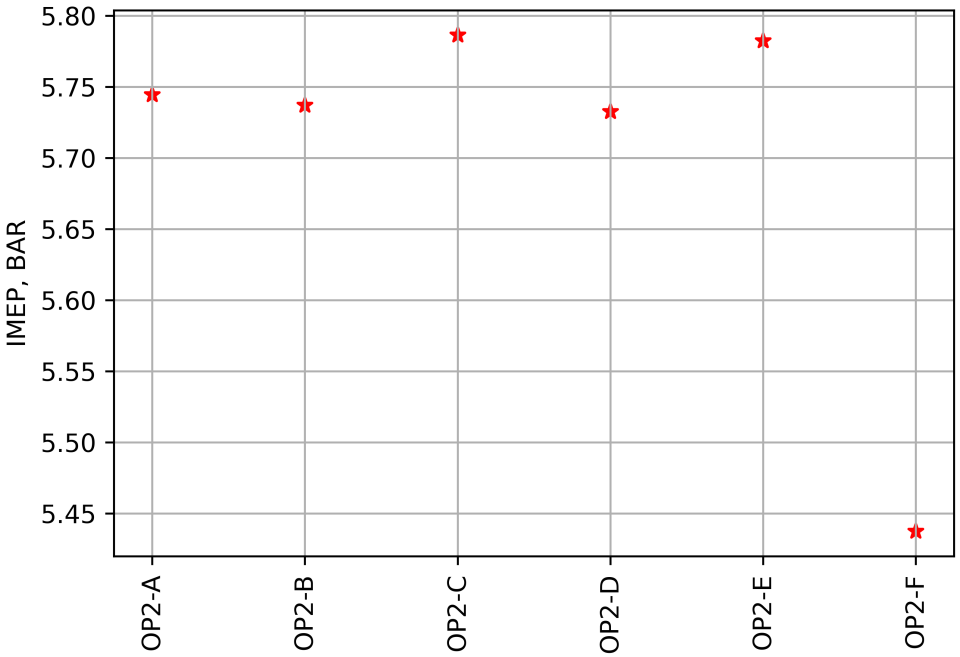

Figure 3: Indicated Mean Effective Pressure calculated for investigated cases in set test 1

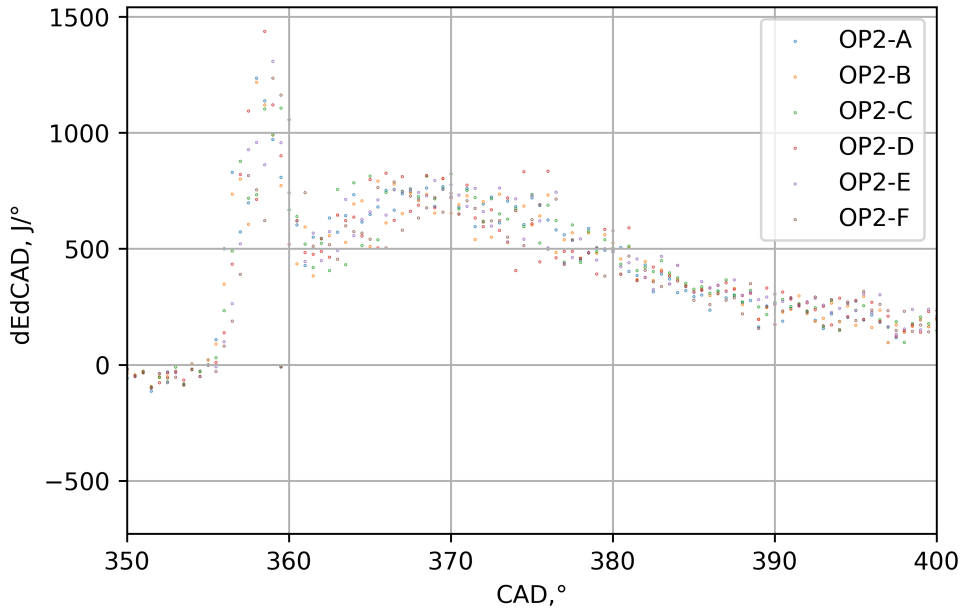

Figure 4: Heat Release Rate calculated during combustion stage in respect to crank angle degree (CAD) for test 1

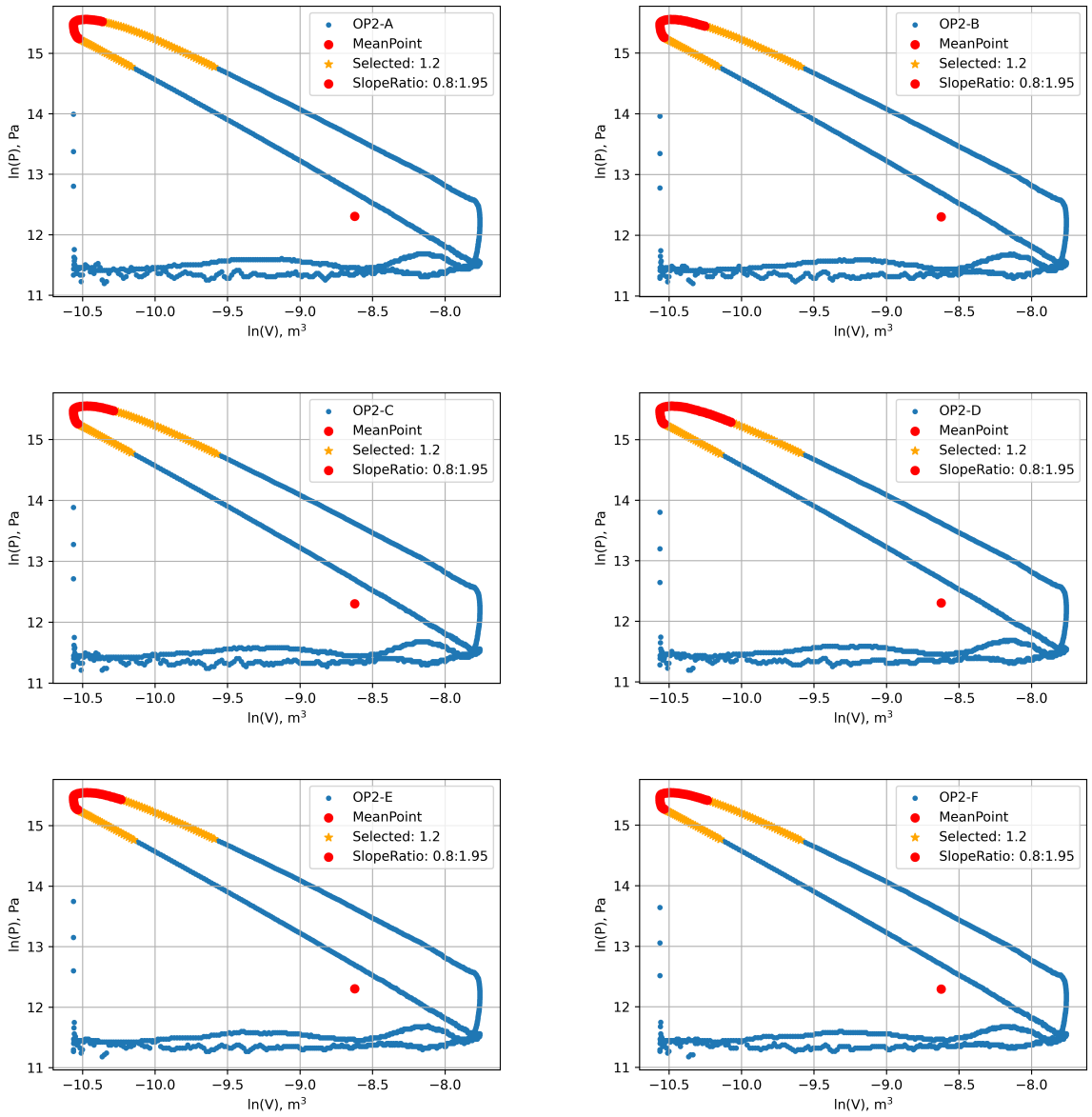

Figure 5: Calculated variation of ln(p) for investigated cases, starting from upper left case A, B, C, D, E, F

A Fourier Transform Infrared Spectroscopy (FTIR) type analiser, manufactered by the company Gasmet (Gasmet DX4000) was used to analyze the exhaust gases composition for analyzed engine working conditions. Various spectrum libraries are embedded in the software that can determine the concentration of each species with an accuracy of 2%. Set of figures listed below shows the extracted from data set emission values with marked STD and FTIR ERROR (2%).

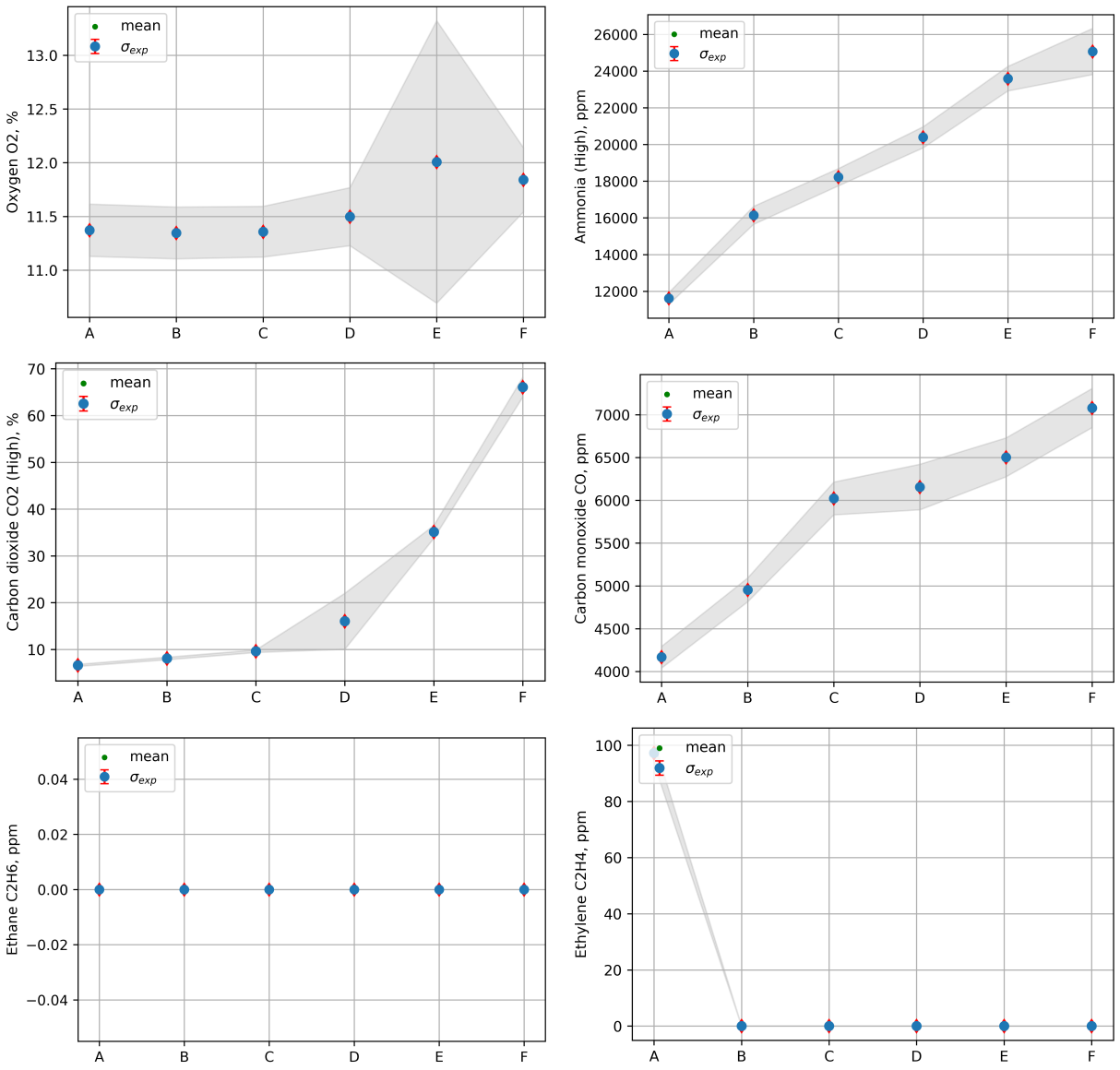

Figure 6: Emission values with marked STD and FTIR ERROR (2%)

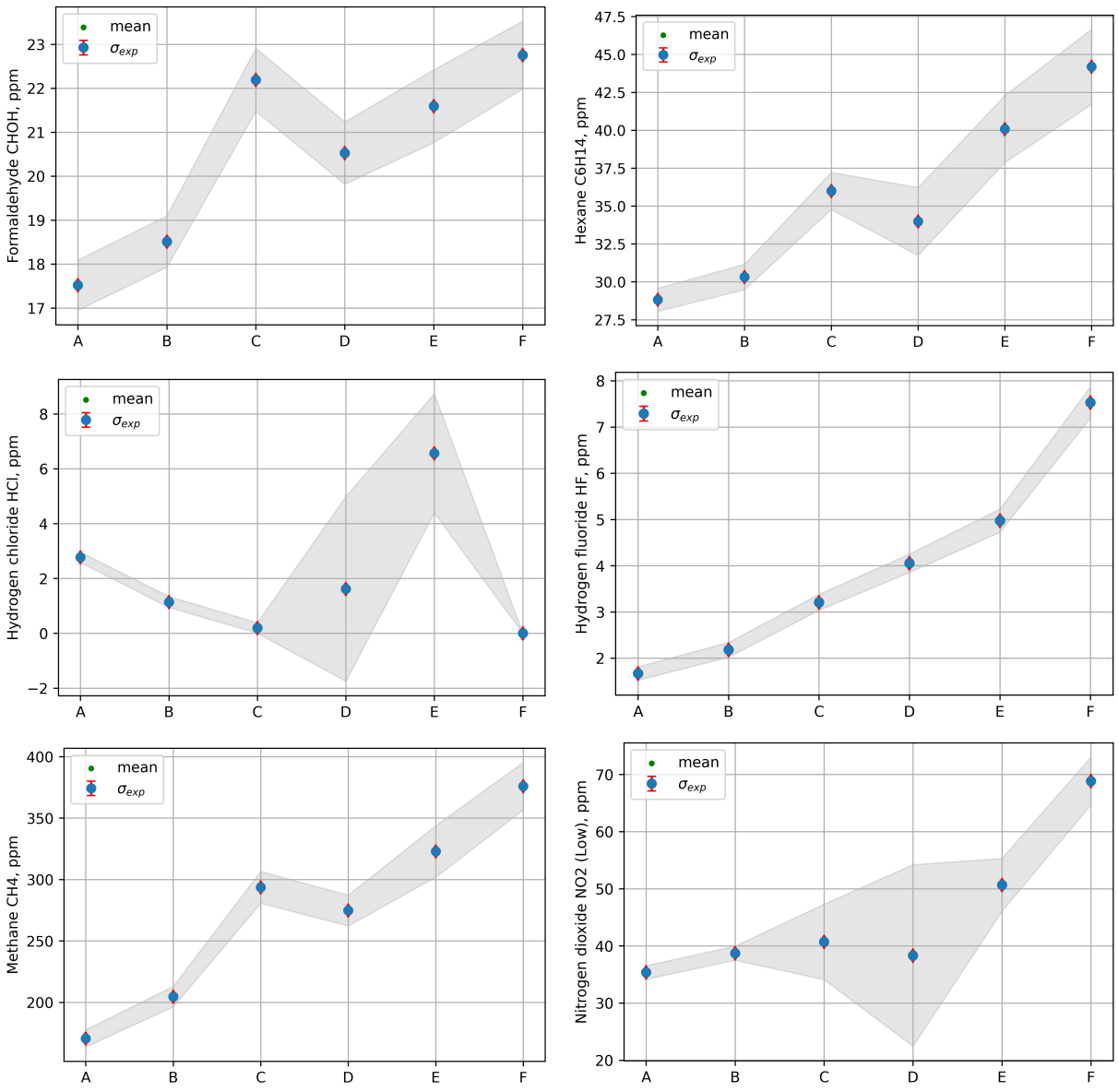

Figure 7: Emission values with marked STD and FTIR ERROR (2%)

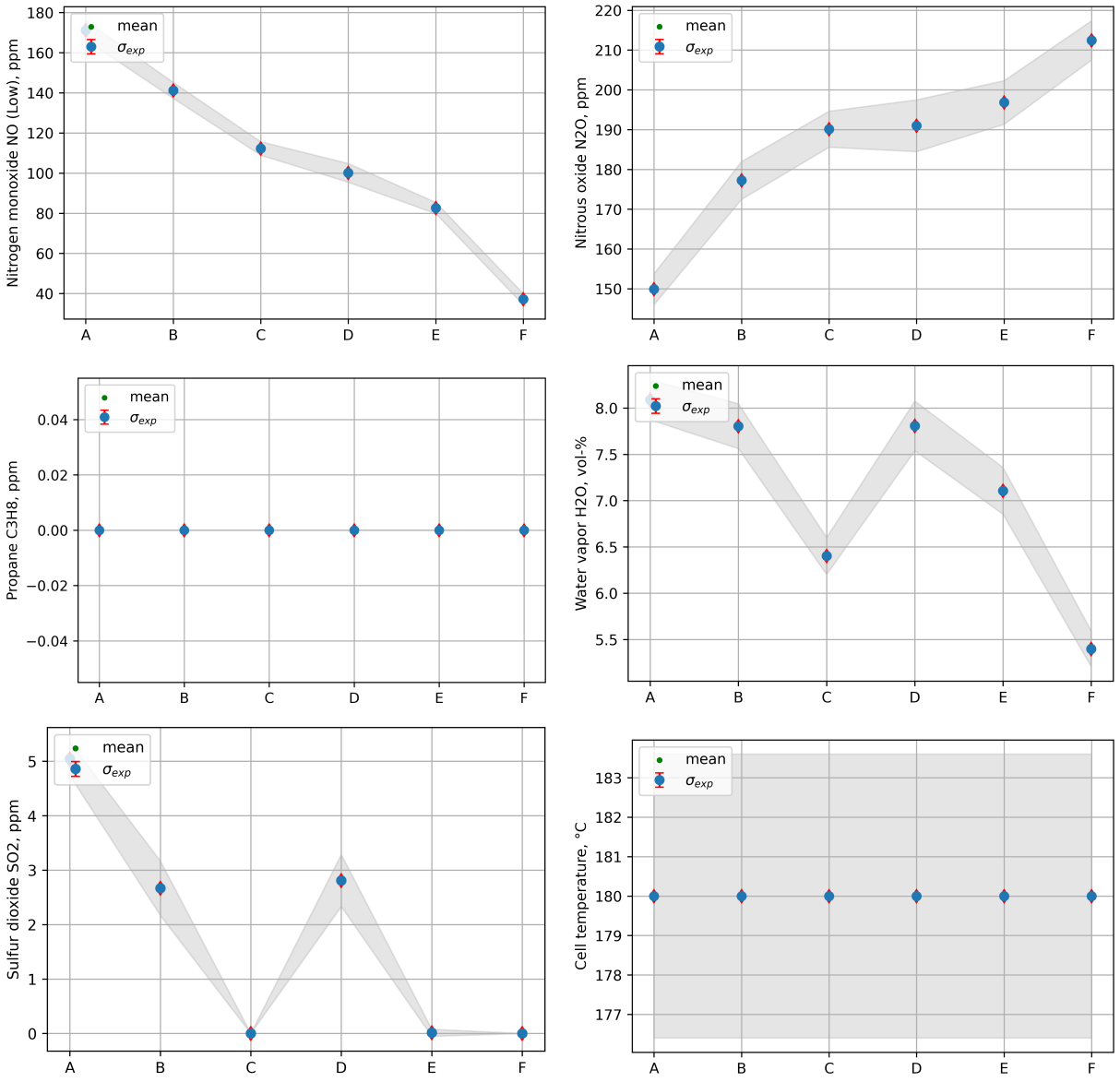

Figure 8: Emission values with marked STD and FTIR ERROR (2%)

1.2 Tractor and engine test at lab environment

A set of tests was performed to simulate the retrofitted tractor operation with different gears selected. The injection timing for ammonia was fixed to 8 CAD bTDC. The operation of the engine was kept at 1500 RPM. Collected engine data is presented in table 3.

Figure 9 shows the calculated Indicated Mean Effective Pressure for investigated AES in combusted fuel. It can be noticed that with increasing AES the IMEP starts decrease. This situation can be mitigated by manipulation of the ammonia and biodiesel injection timing. During carried out test injection timing was fixed, and the engine map settings were to be determined later. Figures 13, 14, 15, 16 illustrate the measured emission for investigated AES of CO_2, CO, NO, NO_2 and NH_3, respectively. Calculated engine efficiency is depicted in figure 10 where it can be noticed that without manipulation of the injection timing the efficiency drops for higher AES. The variation of burned fuels is shown in figure 11. The coefficient of variation of the IMEP is illustrated in figure 12.

The tractor velocity calculated for selected gear and testes AES is shown in figure 17. The calculated emissions of CO_2, CO NH_3 NO_2, NO in respect to the distance in km are presented in figures 18, 19, 20, 21 and 22.

Table 3: Test 2 - engine operational parameters

Name	m_{bio}, kg/h	m_{NH_3}, kg/h	N, kW	IMEP, bar	AES
A	0.437	0.266	2.50	4.98	0.23
B	0.425	0.289	2.46	4.91	0.25
C	0.401	0.334	2.45	4.88	0.29
D	0.374	0.400	2.38	4.74	0.35
E	0.355	0.459	2.22	4.42	0.39
F	0.304	0.509	2.09	4.18	0.46
G	0.297	0.579	2.06	4.11	0.49
H	0.281	0.686	1.97	3.92	0.55

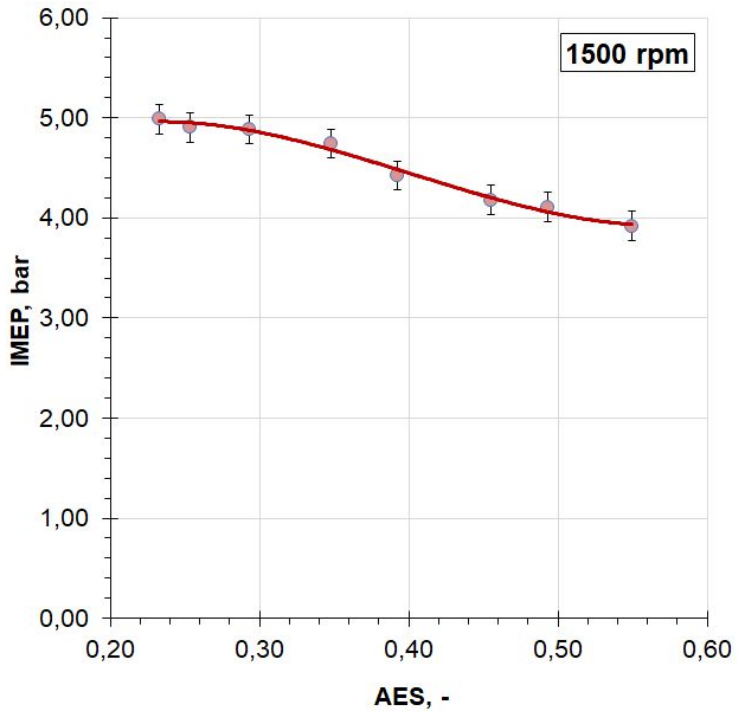

Figure 9: IMEP - Indicated Mean Effective Pressure calculated for investigated cases

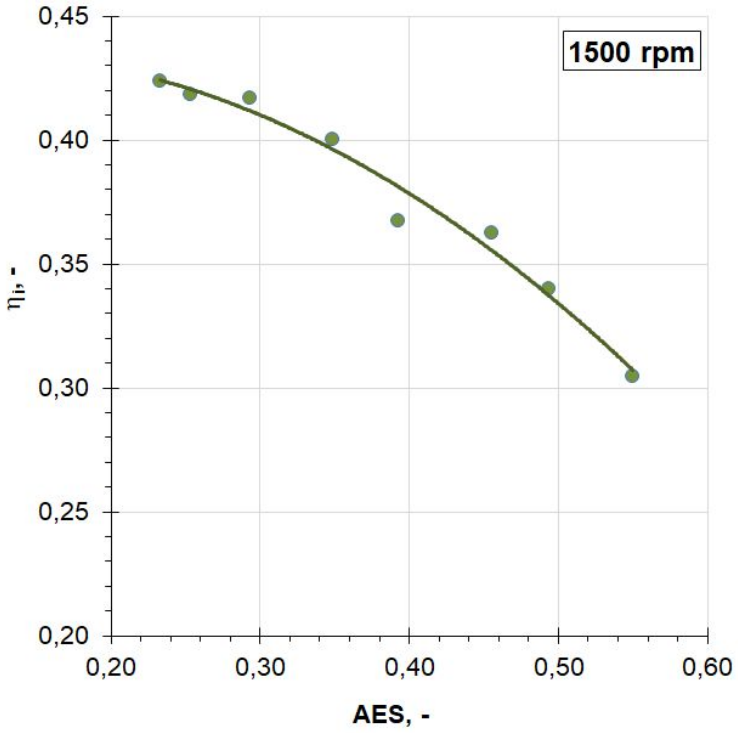

Figure 10: Engine efficiency calculated for different Ammonia Energy Shares

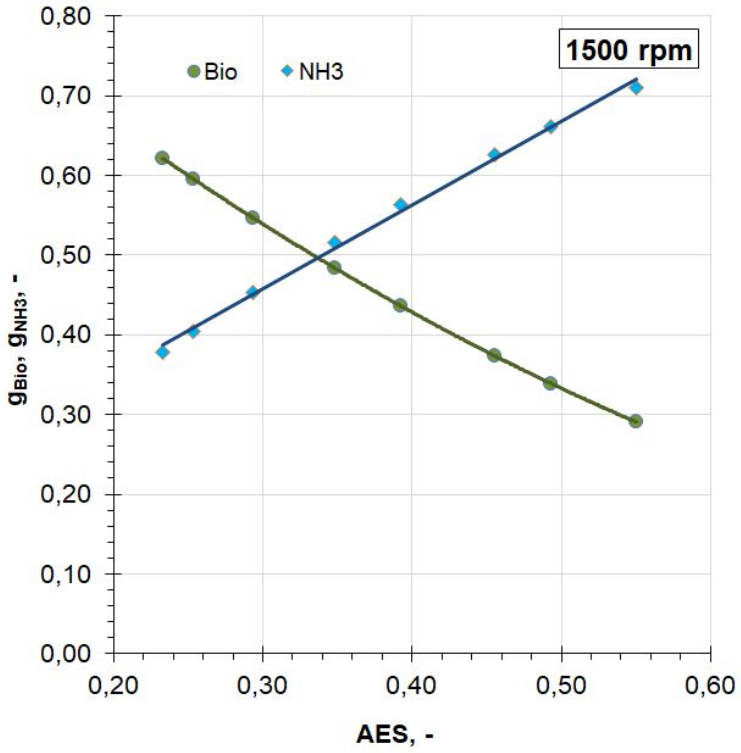

Figure 11: Variation of the fuel ration for different Ammonia Energy Shares

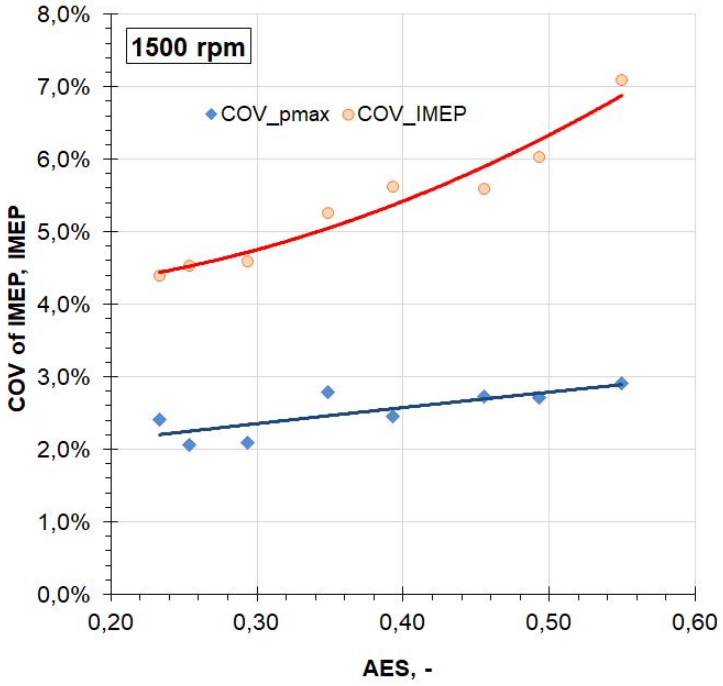

Figure 12: Variation of calculated COV for different Ammonia Energy Shares

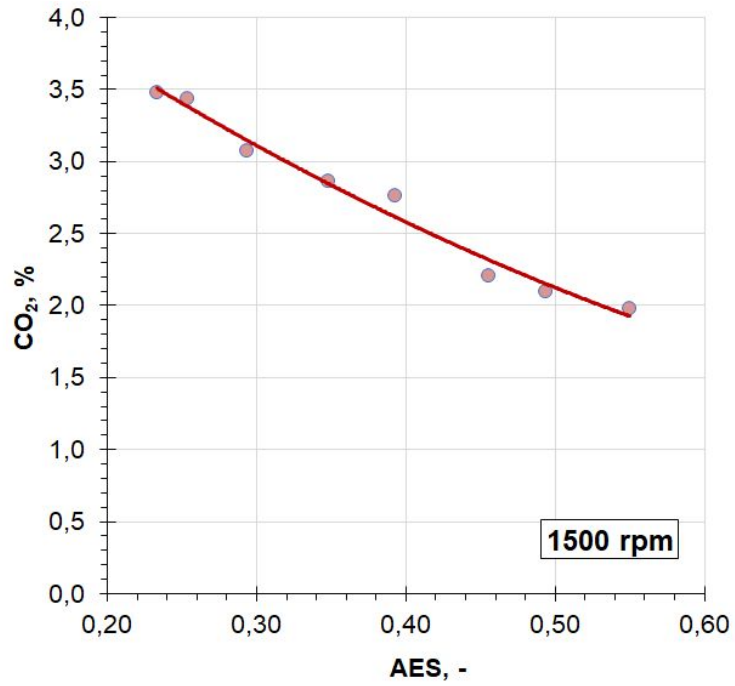

Figure 13: Measured CO_2 emission for different AESs

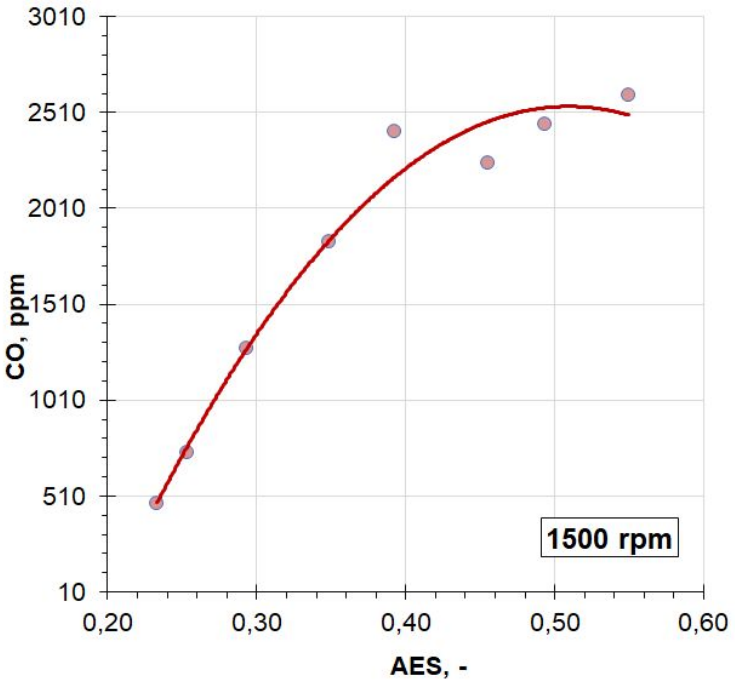

Figure 14: Measured NO and CO emission for different AESs

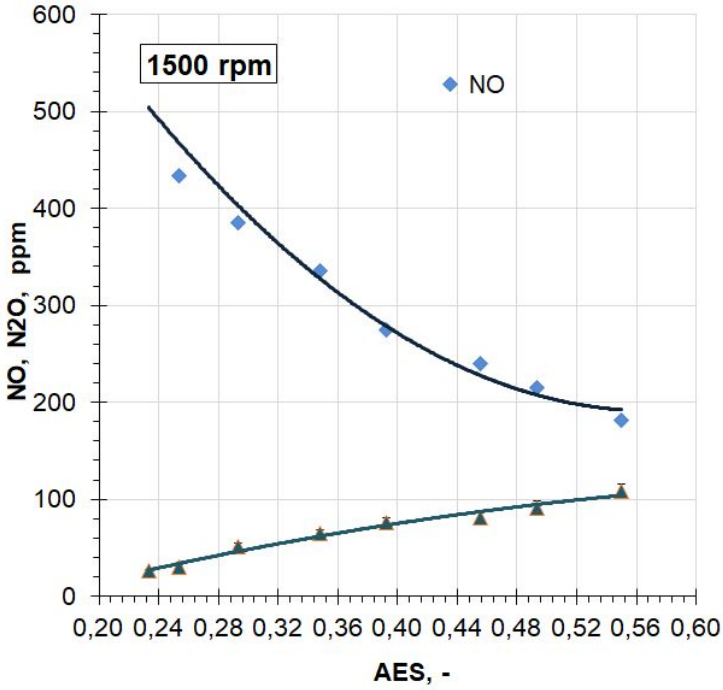

Figure 15: Measured NO and NO_2 emission for different AESs

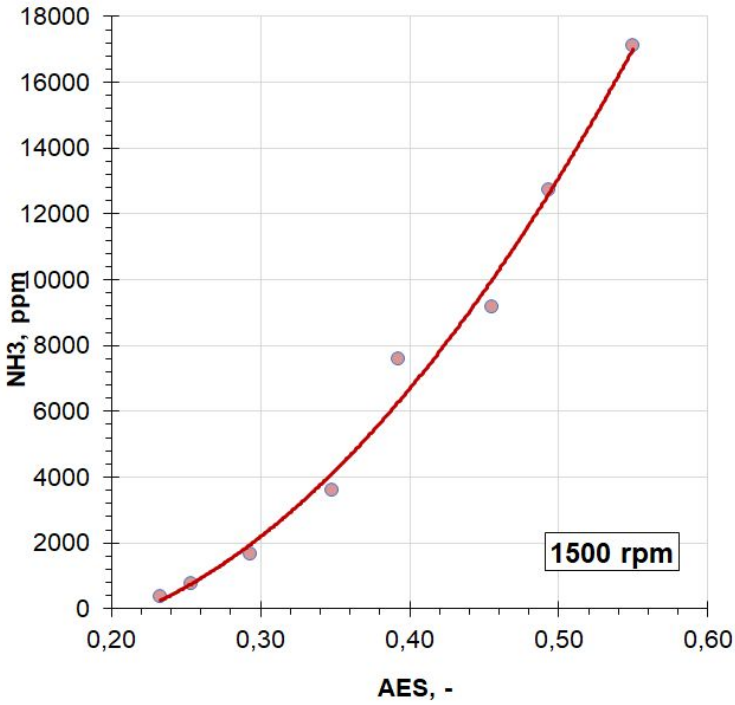

Figure 16: Measured NH_3 emission for different AESs

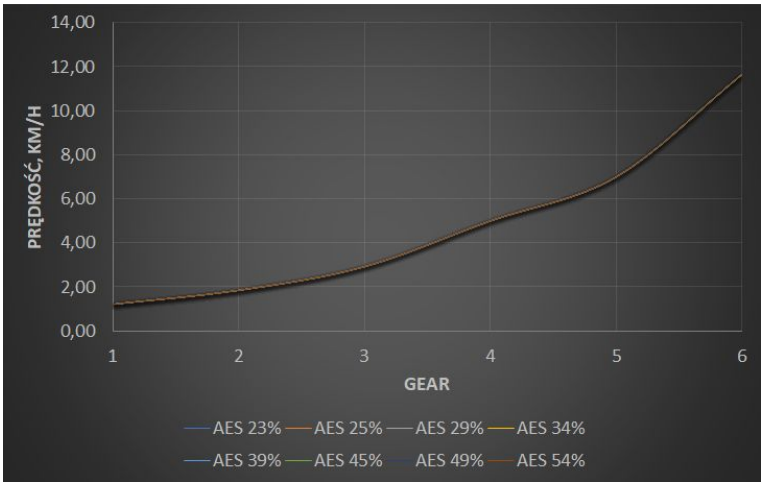

Figure 17: Tractor velocity for different AES and selected gear

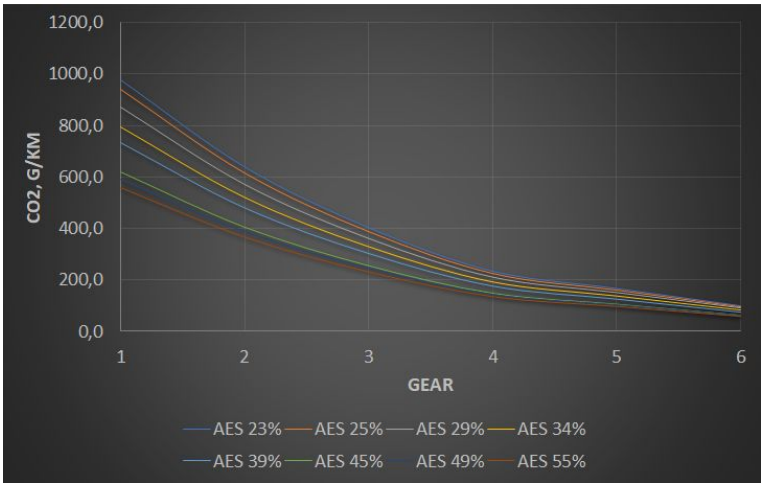

Figure 18: CO_2 emission calculated in respect to distance (km) for different AES and selected gear

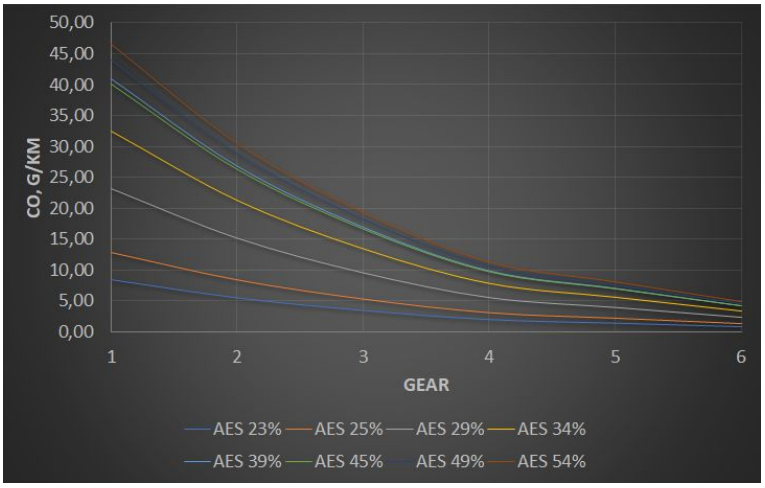

Figure 19: CO emission calculated in respect to distance (km) for different AES and selected gear

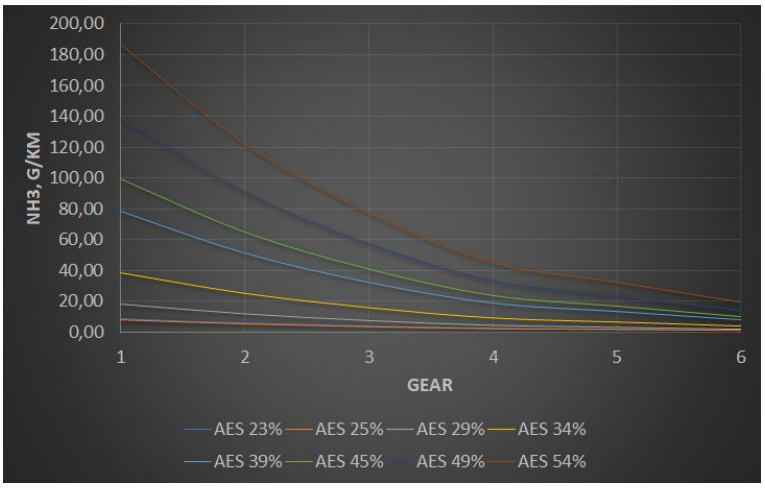

Figure 20: NH_3 emission calculated in respect to distance (km) for different AES and selected gear

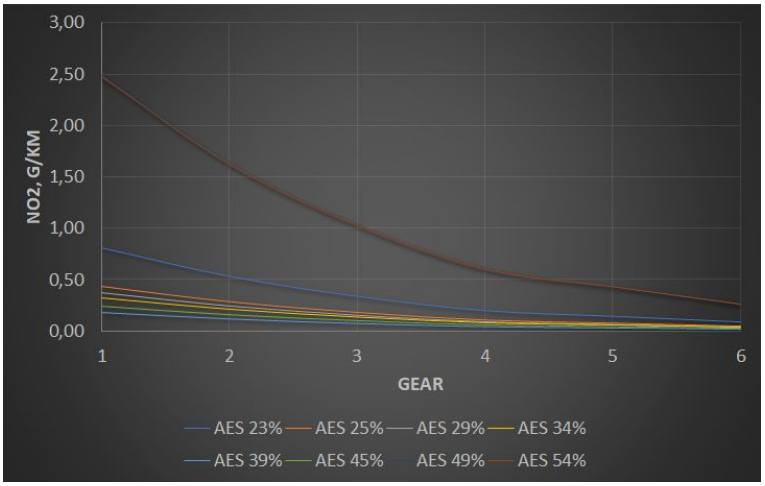

Figure 21: NO_2 emission calculated in respect to distance (km) for different AES and selected gear

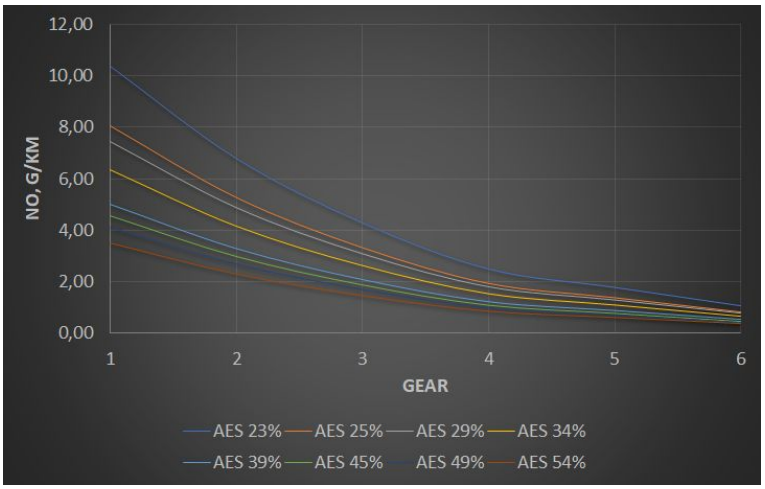

Figure 22: NO emission calculated in respect to distance (km) for different AES and selected gear

2 Engine test using ammonia and biodiesel pilot dose

The engine test rig has been prepared for tests in laboratory conditions using the ammonia fuel line. The air-ammonia mixer has been manufactured and installed in the inlet of the engine. Air-ammonia mixer is a kind of specially designed plate to allow the installation of additional components such as ammonia line, temperature sensor and pressure transducer.

Laboratory tests of ammonia-fuelled internal combustion engine were carried out with a pilot dose of regular diesel and biodiesel. The test has been performed with mentioned earlier port injection of the ammonia to the engine intake manifold. The tests, the results of which are presented below, were carried out at a constant engine speed of 1500 rpm. During the tests, the engine was fuelled by ammonia with a pilot dose of biodiesel and biodiesel only. Figure 23 shows the efficiency of electricity generation as the internal combustion engine was loaded by an asynchronous generator. As can be seen, running an internal combustion engine including biodiesel achieves a slightly higher efficiency comparing to use of ammonia. The reason for the difference may be a constant value of the injection timing of the biodiesel pilot dose. The engine load on the abscissa axis expresses the relative torque of the internal combustion engine.

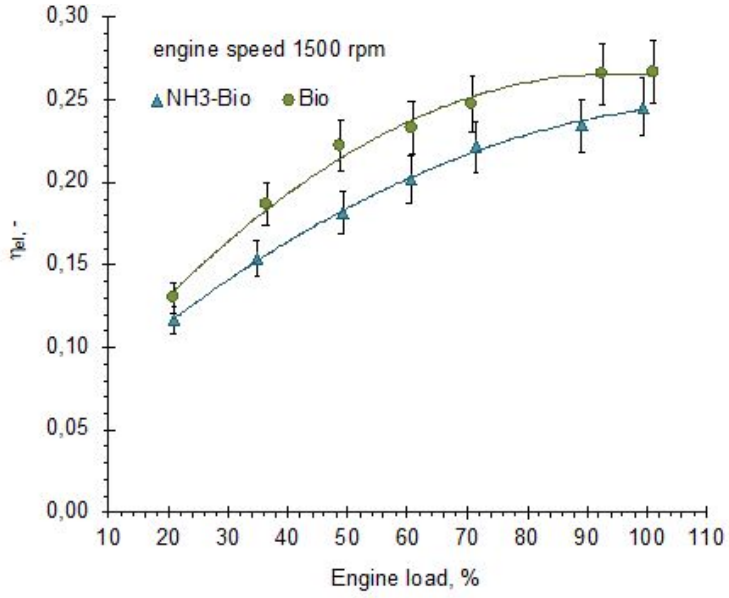

Figure 23: The efficiency of electricity generation

Figures 24 and 25 show the real and stoichiometric AFR (air fuel ratio). Ammonia has a lower specific combustion air requirement. For this reason, the AFR value is lower. The decrease in AFR values as the internal combustion engine load increases (Fig. 24 - real value during engine tests) is due to the increase of fuel dose for higher loads.

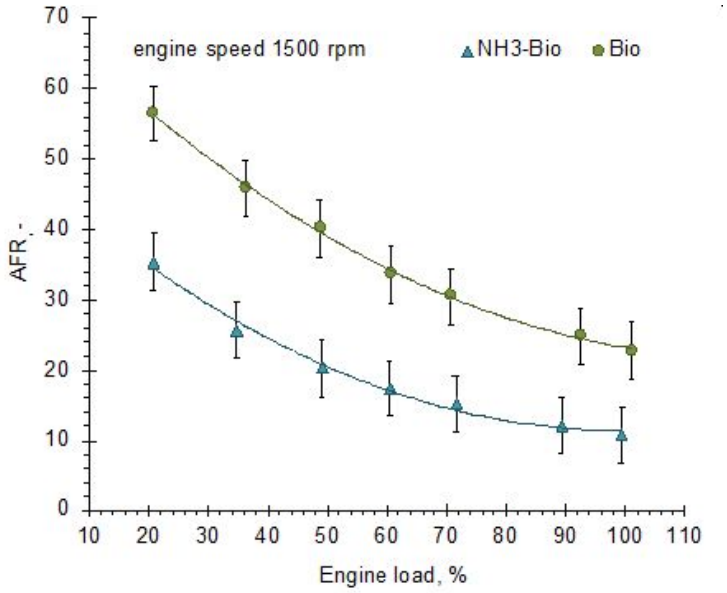

Figure 24: Actual value of AFR

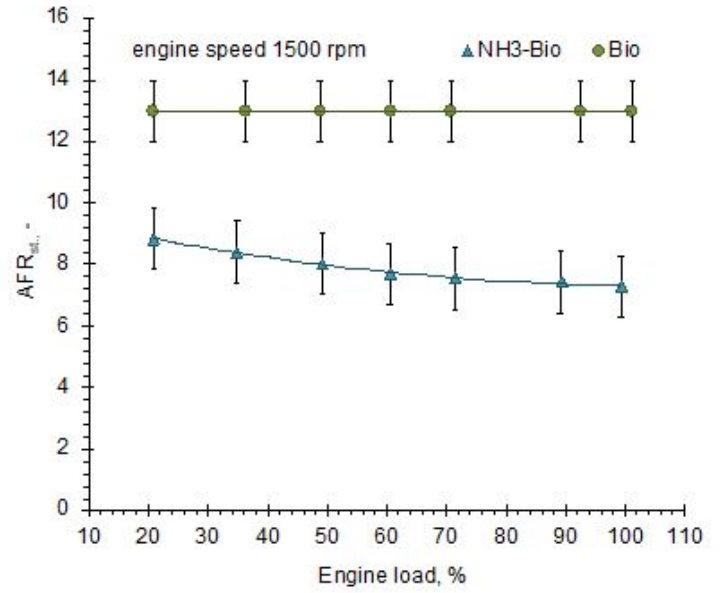

Figure 25: Stoichiometric value of AFR

For theoretical stoichiometric conditions (Figure 25), the decrease in AFR for an ammonia-biodiesel mixture with increasing engine load is due to the changing specific combustion air demand. The pilot dose of biodiesel was constant during the experiments carried out, so the proportion of ammonia in the blend increased as the engine load increased. An increase in the proportion of ammonia results in a higher hydrogen content in the ammonia-biodiesel mixture. This reduces the specific oxygen demand for combustion.

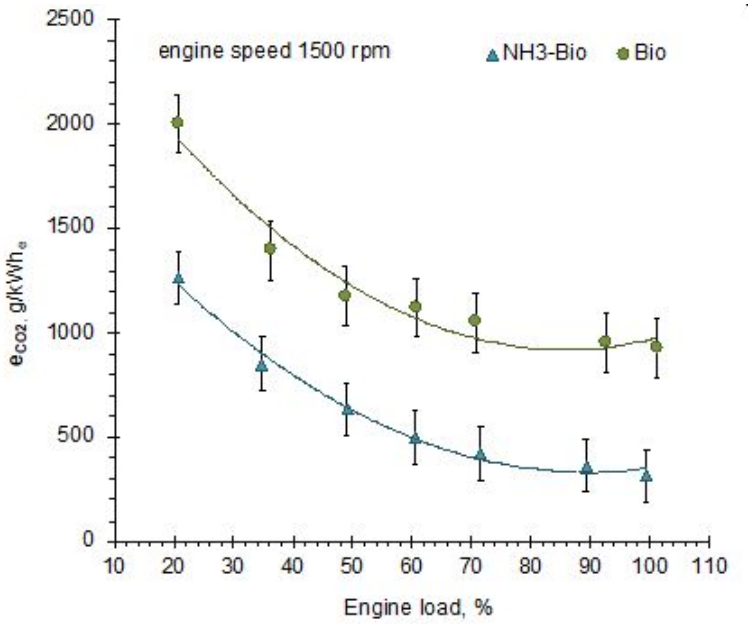

Figure 26: Specific emission of CO2

Figures 26 to 29 show the specific emissions of CO2, CO, HC and NO. As can be seen from Fig. 26, the specific emission of carbon dioxide is lower when burning ammonia with a biodiesel pilot dose compared to only biofuel combustion. The decrease in CO_2 emissions is constant over the entire load range of the engine and its value results from the value of pilot dose of biodiesel used during the tests. Hence, the observed CO2 emissions during ammonia combustion come from the combustion of pilot fuel dose.

Carbon monoxide and hydrocarbon emissions (Fig. 27 and 28) are lower when burning ammonia than when burning biodiesel alone. The main reason for the observed trend is the lower presence of hydrocarbons and the carbon element in the engine cylinder during ammonia combustion.

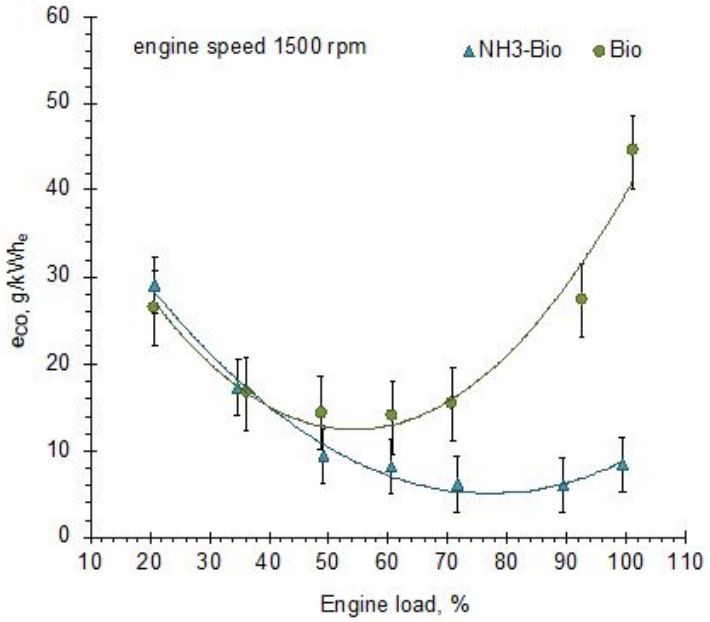

Figure 27: Specific emission of CO

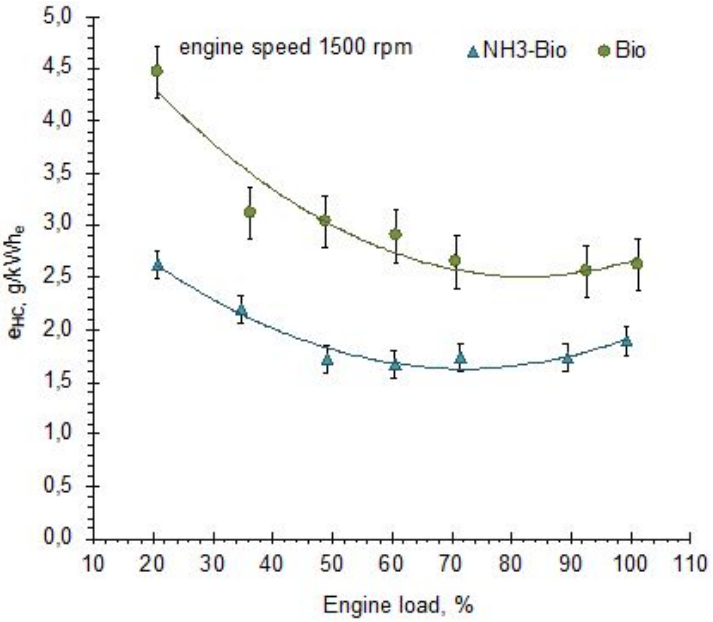

Figure 28: Specific emission of HC

Specific emissions of nitrogen oxides are significantly higher in the case of ammonia combustion, which is mainly due to the nitrogen content of the ammonia fuel, as can be seen from figure 29. In addition, the port-injection method of ammonia supply has its limitations in terms of control of the combustion process and, consequently, of the pressure course and the instantaneous temperature value of working medium in the engine cylinder.

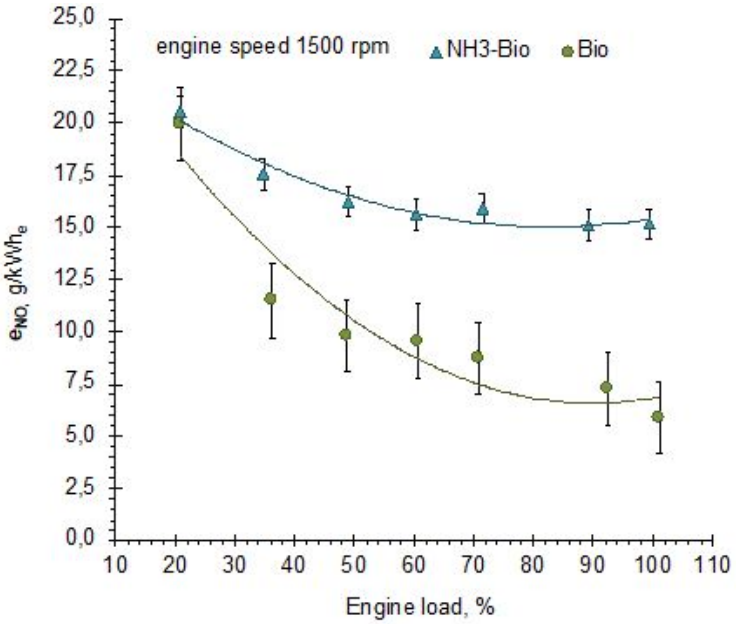

Figure 29: Specific emission of NO

3 Tractor transient dynamic model

In order to facilitate the calculation of the tractors energy usage in real working conditions, a dynamic model of the vehicle has been created in MATLAB Simulink, using Simscape and Simscape Driveline components. The model was based on the data obtained from previous chapter A default example simulation of a vehicle with manual transmission has been used as the starting point, though heavily developed and modified. The model includes:

1. A simplified engine model, using a Simscape engine block.
2. Shafts with inertia.
3. A six gear gearbox with friction losses implemented.
4. A vehicle body model configured for tractor mass and including interaction between wheels and surface.
5. A power take of shaft that can be engaged and disengaged at will, with custom load.
6. A custom gear shift logic system.

The interactions between those elements for a given driver input are calculated dynamically. Data about power, rpm and torques is gathered from every simulation. The user can program driver inputs by using the Simulink signal builder app, setting target velocity and power take-off engagement as time signals. Gear and clutch engagement is automatic according to a certain target values set by the user, which are described in detail in the concerned subsection.

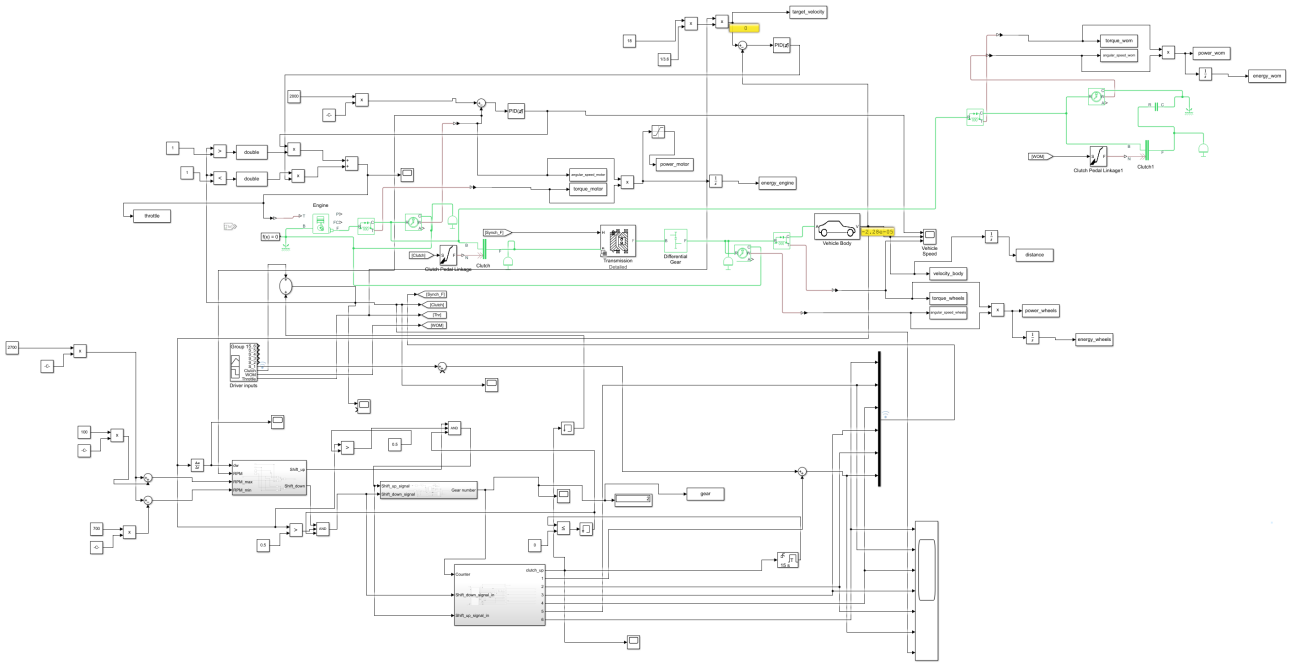

Figure 30: A general schematic drawing of the dynamic tractor model in the Simulink software

For fuel consumption, measurements were taken from the 02.03.2022 dataset (biodiesel fuel) as it contains multiple RPM and torque values, and a regression function has been created in the following form:

$$\dot{m} = aM_e n_e + bM^2 + cM_e + dn_e + e, \mathrm{g/s} \tag{1}$$

where M_e is the engine torque, n_e the rotational speed in RPM and $a = 1.1056 \cdot (10^{-}5)$, $b = 3.8844 \cdot (10^{-}4)$, $c = -1.1850 \cdot (10^{-}2)$, $d = 5.4252 \cdot (10^{-}7)$, $e = 9.4482 \cdot (10^{-}2)$.

The model calculations, that is solving the equations of conservation of momentum and angular momentum are carried out within simulink using the built in ODE23 solver for ordinary differential equations, with a variable time step. The maximum length of the time step is $10^{-}3$ s and the length is chosen adaptively.

The vehicle driveline consists of:

- a mechanical reference point,
- the engine,
- torque and rpm measurement points on the engine side,
- engine inertia,
- main clutch,
- gear box,
- differential gear,
- the vehicle body subsystem,
- power take off connection,
- torque and rpm measurement points on the driveshaft side.

The in-program schematic of the driveline is shown in figure 31. The values of the moment of inertia are for now assumed, and set in such a manner as to smooth the simulated vehicle motion. Real values can be input once the physical vehicle is available. Due to low speeds of the machine it is assumed however that the influence of these parameters is not significant.

The engine is modelled based on the data of maximum torque from measurements, the torque and rpm is calculated dynamically by a built in 3rd order polynomial model. Peak power has been set at 5111 W, at 2897 rpm. Stall speed is set at 700 rpm, and red line speed, that is the speed at which the throttle will be automatically limited has been set at 3000 rpm as was done during engine mapping.

A clutch connects the engine with the gearbox and the rest of the system. This has been modelled as built in "Loaded contact rotation friction" module. The clutch requires a force to disengage, and the force threshold is 120 N. The force "signal" can be either generated manually by the "Signal builder" or come from the shift logic module.

Mechanical friction, as obtained from measurements has been implemented in the model within the gearbox module, to reflect its dependence on the gear selection.

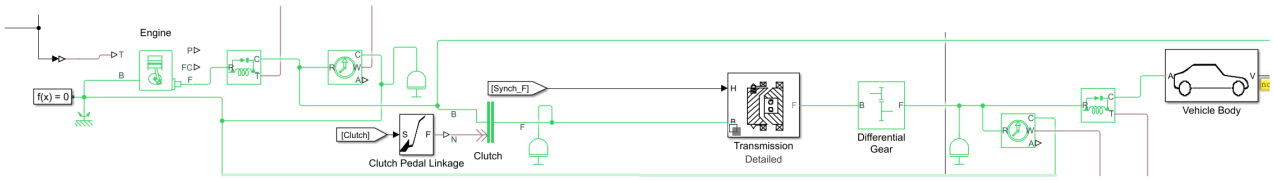

Figure 31: Main vehicle driveline

The transmission has been modelled as a set of simple gears, with gear ratios corresponding to those on the real tractor, that is:

1. 1/145,
2. 1/95,
3. 1/60,
4. 1/35,
5. 1/25,
6. 1/15.

Friction losses correspond with each gear separately (see fig.32). From the measurement results, the friction torque was calculated using the wheel shafts as a reference. It was found, that the characteristic of this torque as a function of the wheel rotational velocity was linear. This has been implemented into the model by rotational friction modules, which accept such linear functions as an input. The gears are modelled as engaged by a combination of dog and cone clutches as a synchronized gearbox (fig.33). This necessitated a certain deviation from reality, as to make solution possible, the "friction" modules have to be engaged separately by their own sets of clutches. This is shown in fig.34.

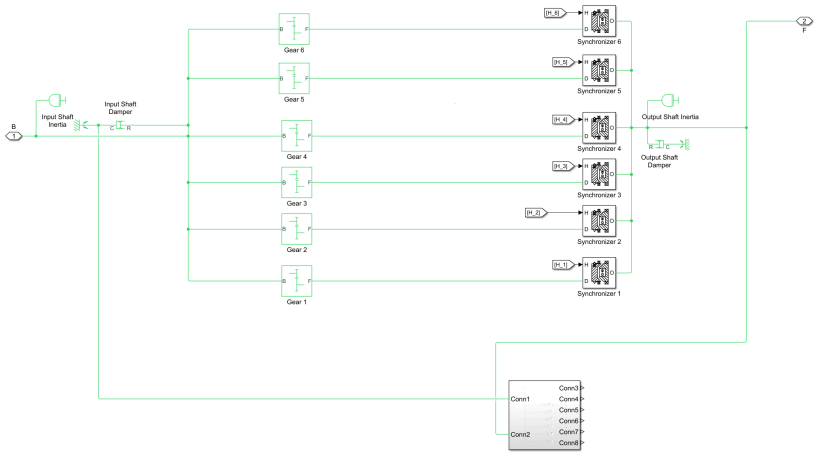

Figure 32: Transmission model general schematic

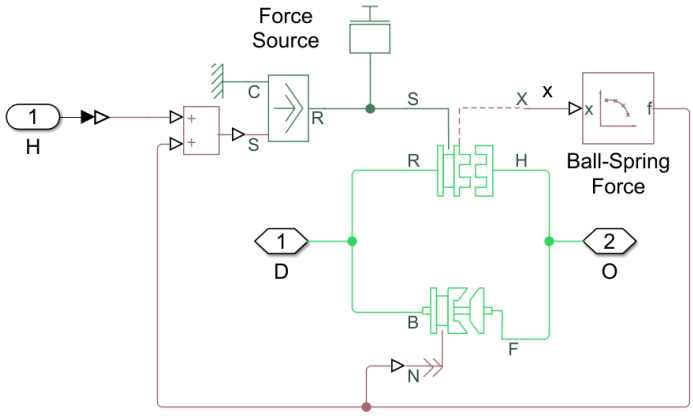

Figure 33: Synchronisers composed of dog and cone clutches

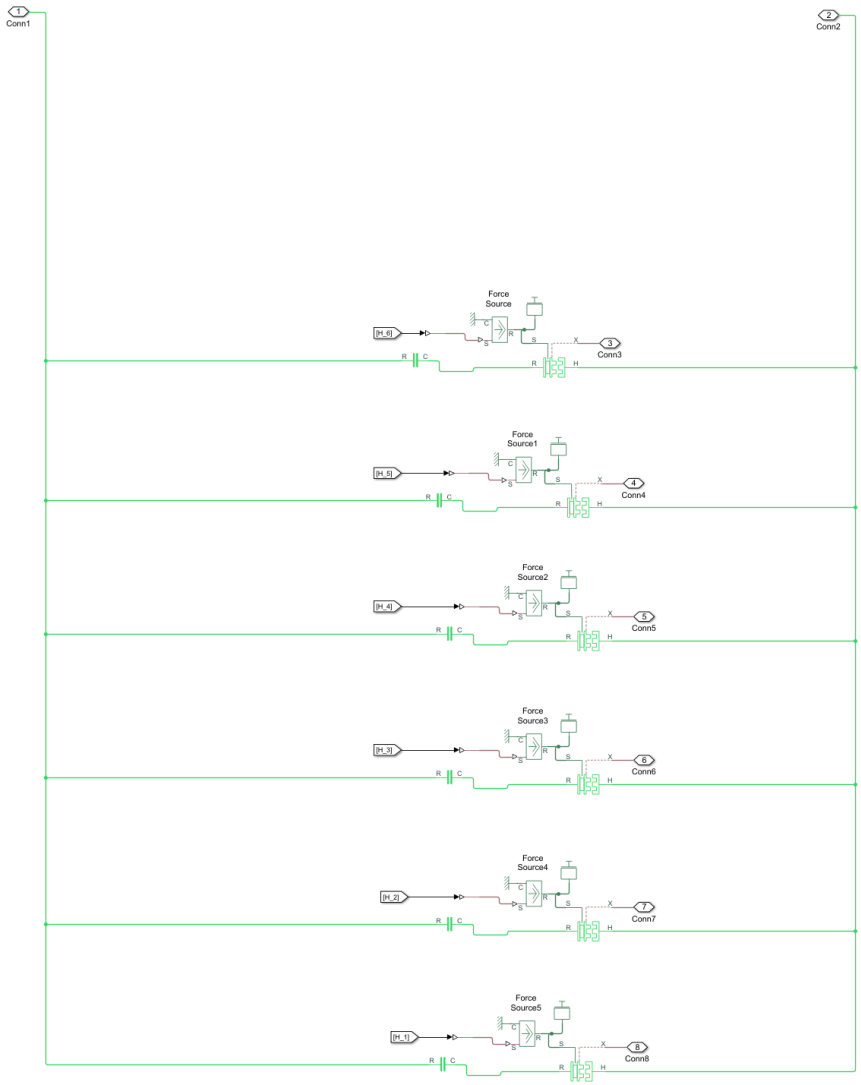

Figure 34: Friction modules for the gearbox subsystem

The friction is calculated as:

$$M_{fr} = M_c + \mu_M \omega_w, \tag{2}$$

Where M_c is the Coulomb friction torque, in the model assumed as the constant component of the linear friction function derived from measurements, and μ_M is the viscous friction coefficient, here taken as the first term coefficient of the same linear function. ω_w is the angular speed of the wheels. The values of the coefficients are shown in table 4.

Table 4: Friction coefficients for each gear as derived from measurements

Gear	M_c	μ_M
1	12.38	92.07
2	38.51	93.15
3	16.79	70.77
4	27.74	8.03
5	23.84	4.60
6	19.47	3.16

To model the body of the vehicle a default Simscape Driveline block is used. The vehicle body block allows for the input of the vehicle mass (used to calculate friction and inertia), the drag coefficient (0.5912 based on the measurements) and incline angle. This is coupled to two "wheel" modules responsible for interaction with the surface. Whithin the wheen blocks the inputs include the diameter (0.68 m) and the rolling resistance (0.14, as used within other project reports). The subsystem is shown in fig. 35.

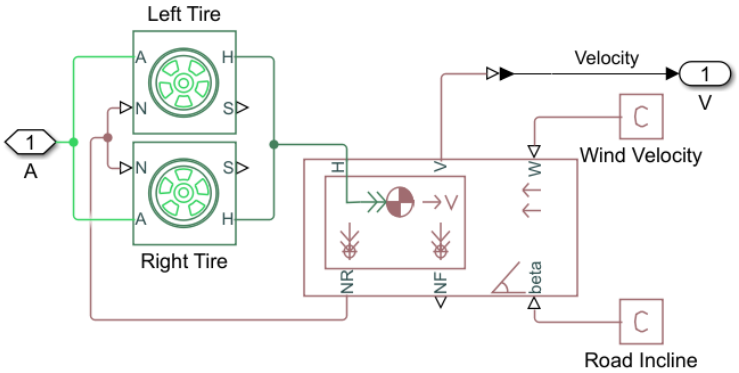

Figure 35: The vehicle body subsystem.

Power take off is modelled as a separate shaft, engage from the engine via a separate clutch. The clutch is modelled in exactly the same manner as the main drive system clutch and controlled by a signal set by the user. This allows for the external device to be powered within a desired time period.

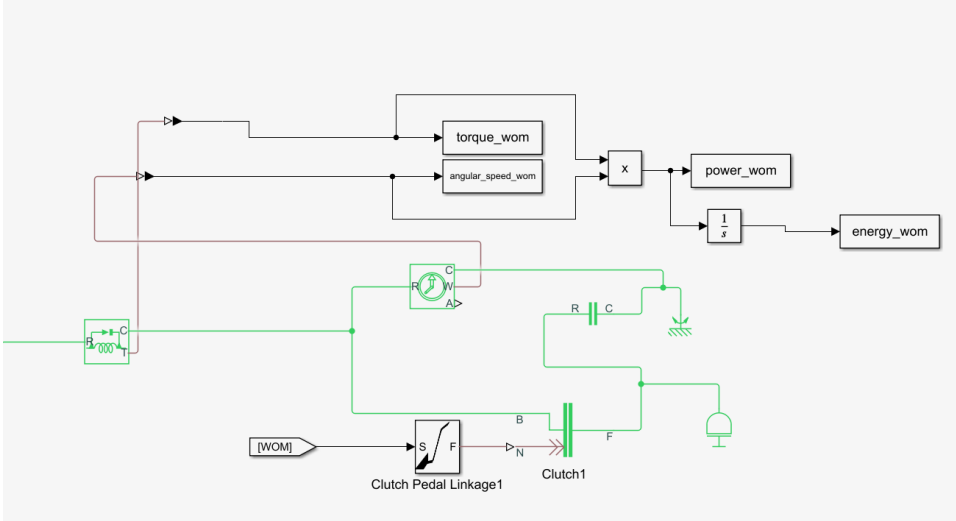

Figure 36: Power take off subsystem

The load of the PTO is modelled as the "rotational friction" block, and the friction torque can be set by the user, to mimic the behaviour of the desired machine.

In its most basic form, the model could accept inputs in the form of time signals responsible for the control of the engine throttle, clutch, gear box and PTO. However data that could be provided to those inputs is difficult to acquire, especially without field test results. For this reason, it was decided to implement a logical system, using simulink components, allowing for the effective automation of the virtual tractor. In this system only the signal for the PTO is a pre-defined input, while the others are calculated within the model in such a way as to achieve a desired speed of the vehicle. The speed is supplied by the user as a time signal, within the range of values from 0 to 1, corresponding to the fraction of the maximum speed set by the user. The simulation starts with the tractor in idle. Afterwards there is a pre-defined sequence of signals, corresponding to the shift into first gear. After reaching a pre-defined minimum speed (set as 5 m/s), the simulation continues automatically. The driver input consists of two main subsystems - motor control and shifting control. Both work in conjunction and signals are exchanged between the two.

The engine throttle is controlled by the means of two Proportional-Integrating-Differential controllers. The first can be called the "idling control", and its task is to maintain constant RPM with the clutch disengaged. The desired idle RPM can be set by the user. The regulator measures the difference between the set RPM and the actual RPM and adjusts the throttle accordingly, based on the formula:

$$u(\tau) = K_p(\tau) + K_i \int_0^{\tau} e(\tau)\mathrm{d}\tau + K_d \frac{\mathrm{d}e(\tau)}{\mathrm{d}\tau}, \tag{3}$$

where $u(\tau)$ is the control signal (throttle input), $e(\tau)$ is the error, and K_p, K_i and K_d are the proportional, integral and derivative coefficients derived from regulator tuning. The tuning in the case of this model was carried out automatically. The idle control regulator signal is only routed to the engine if the clutch signal is positive (that is, the clutch is disengaged).

The second controller is the speed control, also implemented as a PID regulator. This regulator sets the throttle based on the error between the vehicle speed and the desired speed signal (set by the user), and is active when the motor is in gear.

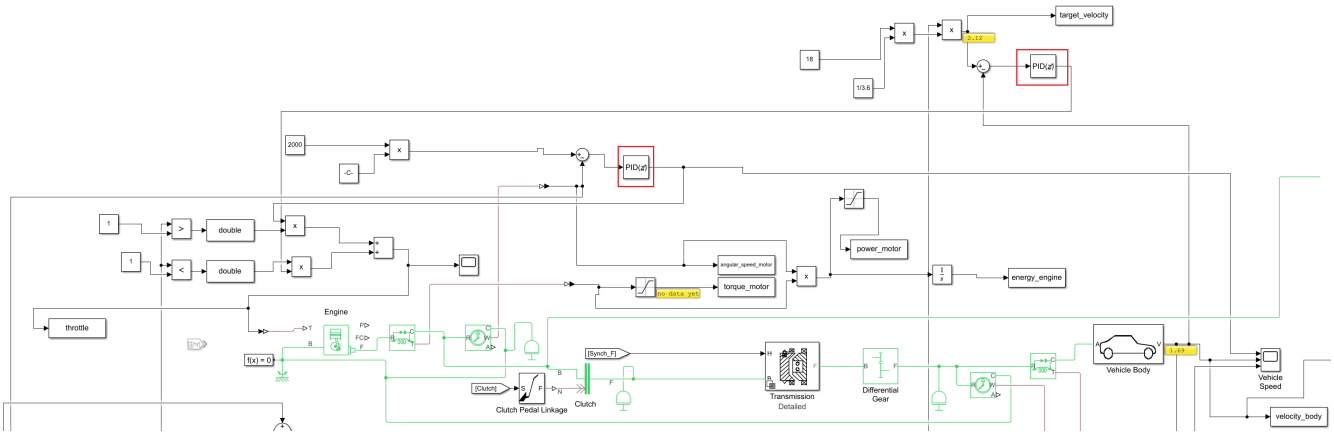

Figure 37: The motor control circuit with the regulators highlighted in red

The gear shift control is much more complex due to the task before it. First of all, it needs to provide a sequence of signals; disengage the clutch, provide force on the synchronizer of the active gear to disengage, provide force on the synchronizer of the required gear to engage, engage the clutch. Second of all, it must select which gear to disengage and which to engage. Third - it must do so in a manner consistent with common driving behaviours, that is maintain the RPM of the engine within a desired range, not stall the engine and not stall the vehicle. It also needs to activate when certain conditions are met, in order to help the vehicle keep up with the speed requirement and to provide smooth acceleration.

It was thus decided, that the gear shifting algorithm will be based on the following inputs:

- vehicle speed
- engine rpm
- vehicle speed first derivative
- maximum engine rpm
- minimum engine rpm
- current gear number
- time from last shift

The algorithm has the following design. If the engine speed reaches maximum RPM, and the vehicle speed first derivative (acceleration) is above a certain threshold, a signal pulse is generated by a dedicated subsystem (block 1 in fig. 38). This pulse is detected by a gear counter (block 2 in fig. 38) and added to the current gear value (displayed in block 4 in fig. 38). Simultaneously, the pulse activates the generation of the shifting signal sequence (clutch, and synchronizer engagement forces) and it is routed to the correct ports based on the counter (this is done in block 3 in fig. 38). Also, a separate signal is generated (triggered by the clutch signal) which has the duration of 15 seconds - if detected it prevents further shifting. This is to prevent the system from engaging two gears at once.

Likewise, for downshifting, the procedure is the same only triggered by reaching a minimum RPM and a set threshold of vehicle deceleration. The shift logic circuit is shown in fig. 38.

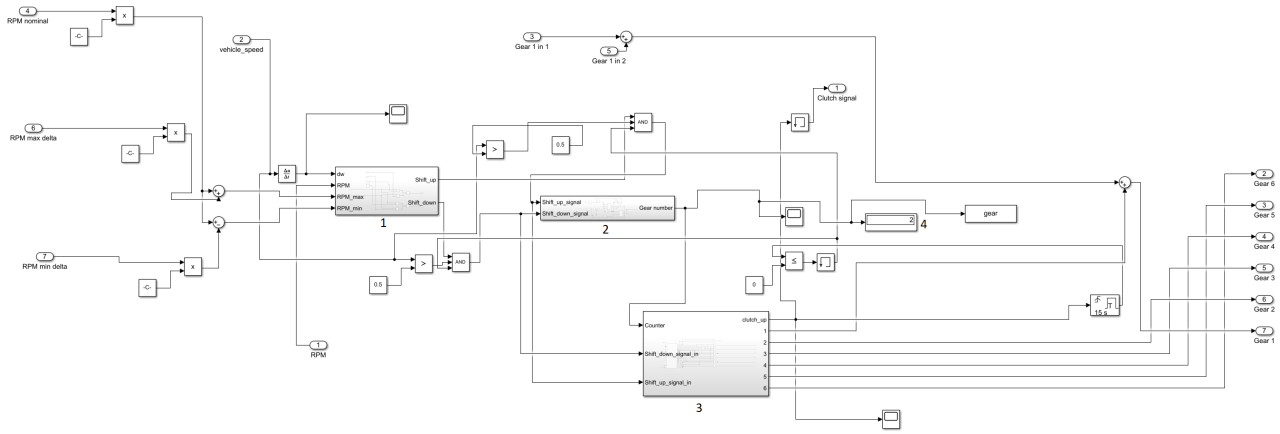

Figure 38: The simulink circuit of tractor shift logic. 1 - shifting pulse generation subsystem, 2 - gear counter, 3 - shifting signal generator subsystem, 4 - gear display

The shifting pulse generation subsystem is shown in detail in fig. 39. It is built from relational operators and accepts the signals in the form of vehicle speed after differentiation, the engine rpm and the rpm threshold values, which are set as constants outside the block.

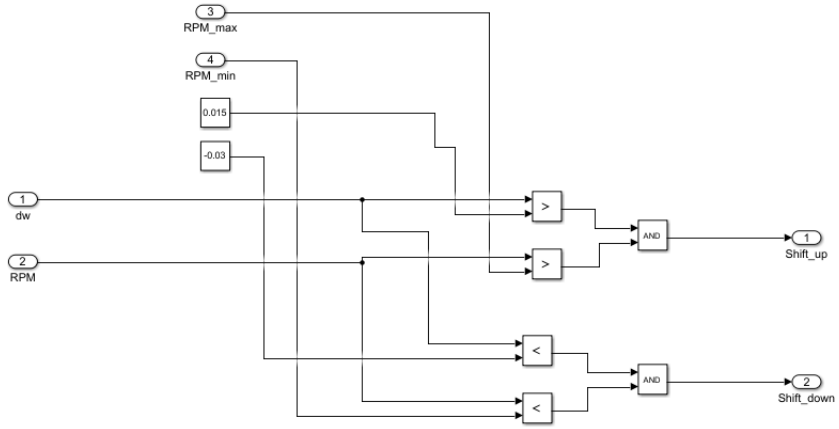

Figure 39: Shifting pulse generation subsystem detailed view

The shifting signal generator subsytem is shown in detail in figures 40 and 41. The first drawing shows the outer layer of the subsystem. The inner blocks are themselves composed of a signal routing

system (not shown) and a signal generator shown in the second figure. The subsystem is responsible for the detection of shifting pulses, and producing the sequence of signals for shifting the gears in and out as well as engaging the clutch. Those signals are then routed based on the input from the gear counter by the use of logic gates and relational operators.

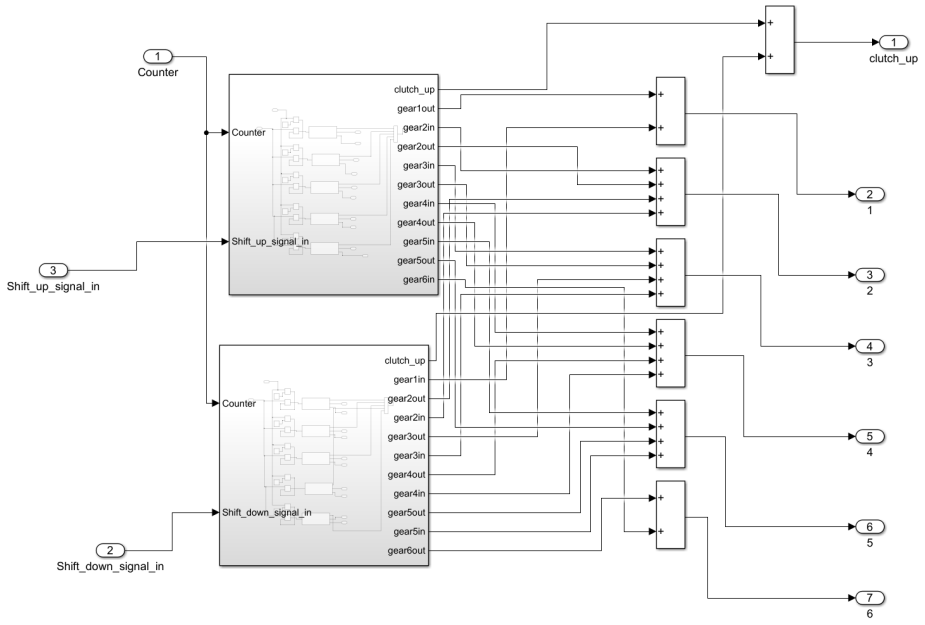

Figure 40: Shifting signal generator subsystem "outer layer" view

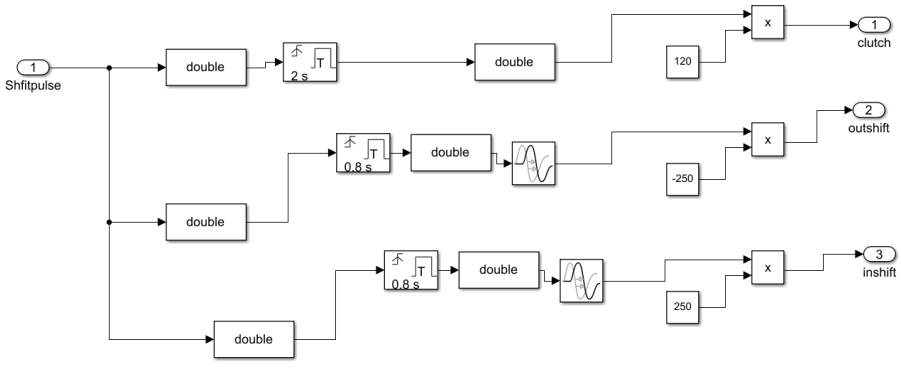

Figure 41: Shifting signal generator "inner" signal generation subsystem

The parameters used by the gear shift logic system, such as the rpm and velocity derivative thresholds could be made subject of optimization in order to arrive at the most economical and efficient gear shifting strategy. They could also be made variable or dependent on other parameters for further optimization.

Simulations have been carried out for certain sets of tractor working conditions, that is for certain time periods, desired speeds and periods of PTO engagement.

For thie first simulation the driver demand is as follows; first the vehicle travels with the speed limit set to 18 km/h, gradually accelerating, after a period of 200 seconds the PTO is engaged and the desired speed drops to 7.6 km/h. The PTO friction torque is assumed as 1 Nm, constant. In the end of the simulation the tractor is to come to a stop by engine braking. A plot of target velocity, actual simulated velocity and the engaged gear is shown in fig. 42.

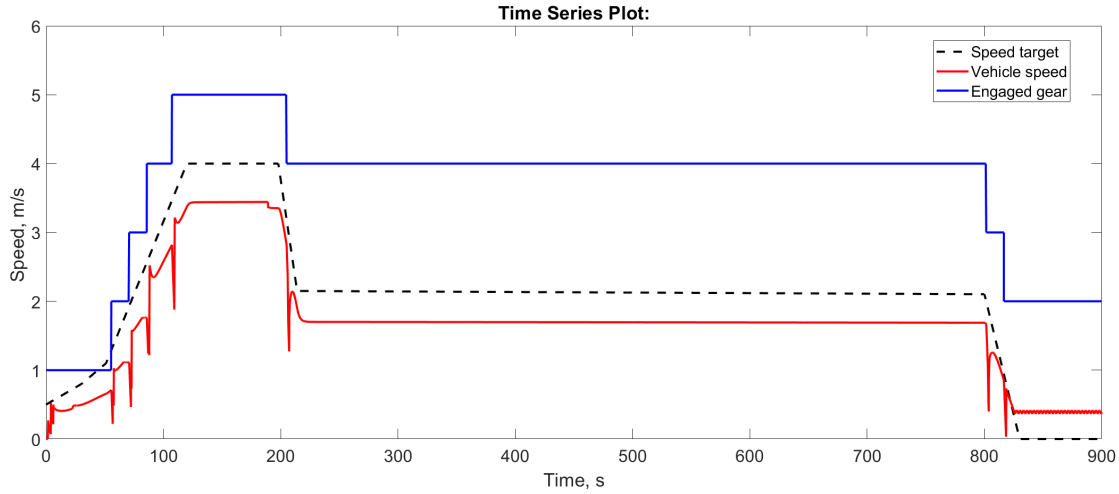

Figure 42: Simulation no.1 velocity and gear plot

Power produced by the engine and consumed by the wheels and the PTO has been shown on figure 43. Torque and RPM of the engine shaft is shown in fig. 44.

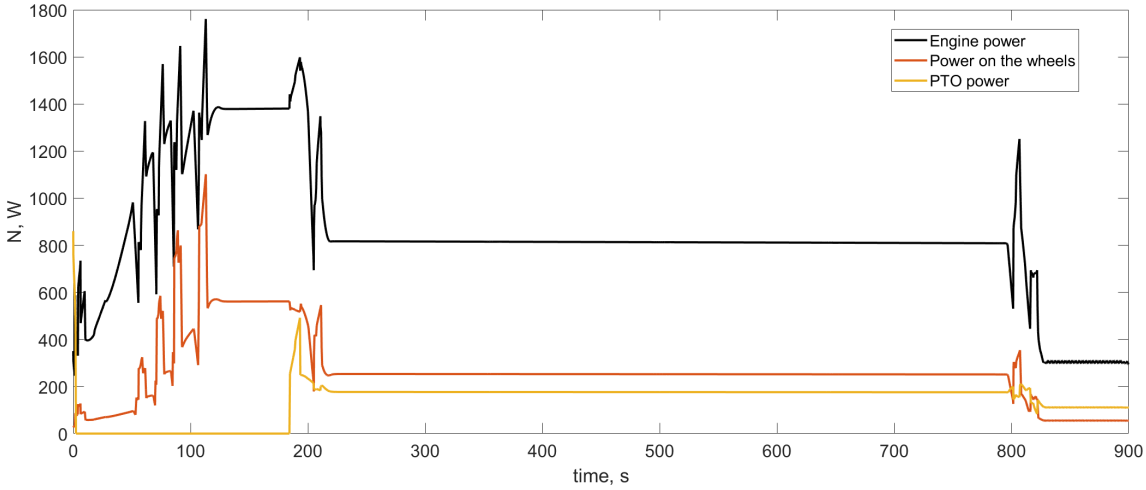

Figure 43: Power plot for simulation no.1, showing power as measured on the engine shaft, wheel axle and the PTO

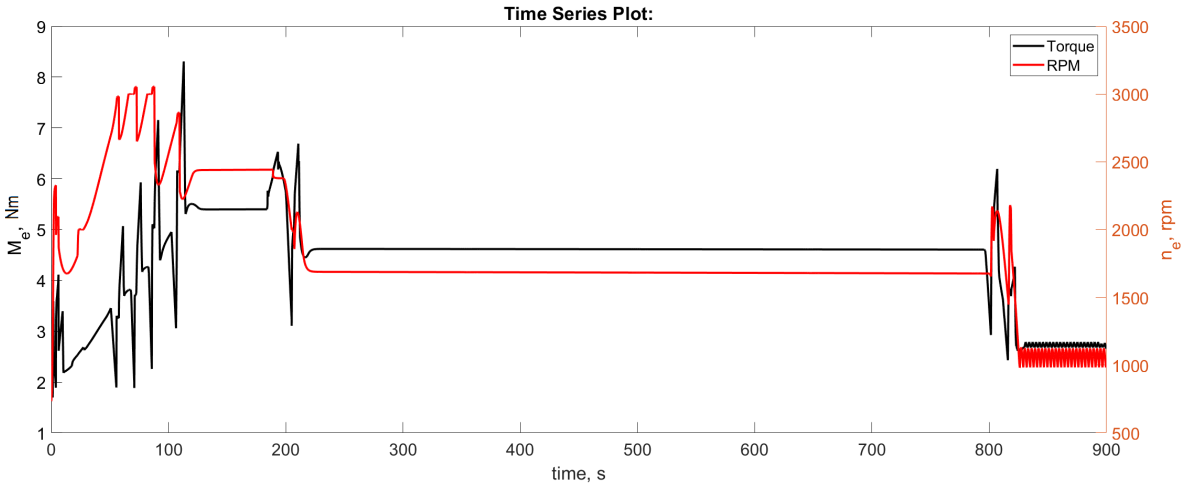

Figure 44: Engine torque and rpm time plots for simulation no.1

Finally, to conclude the energy balance, integrating the instantaneous power and fuel consumption values enables the ploting of overall energy production, consumption and fuel usage as a function of time. This is shown in figure 45.

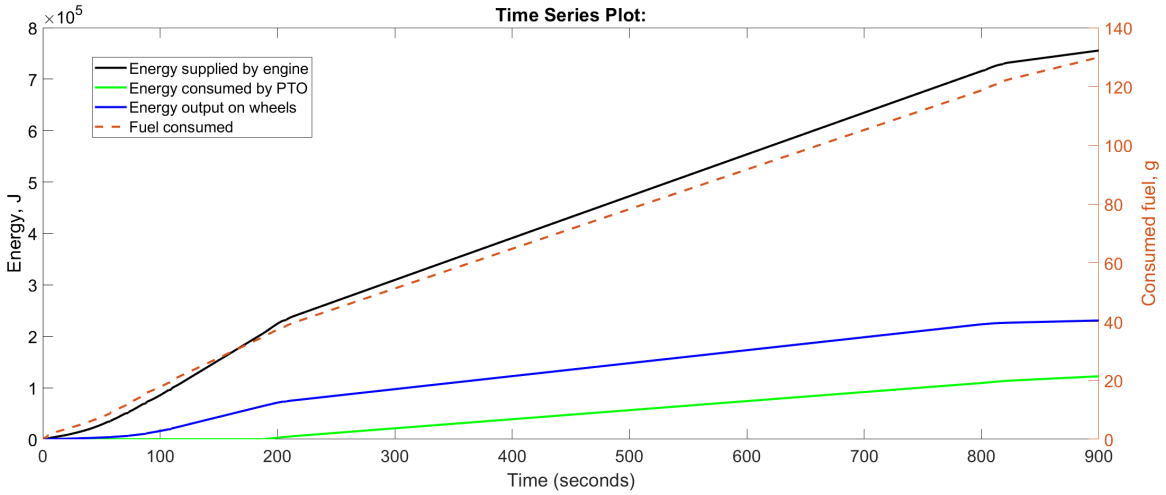

Figure 45: Energy production, consumption and fuel consumption plot for simulation no.1

Overall the distance travelled was 1.51 km and the fuel consumed was 129.91 g.

In the next simulation, the tractor is set to gradually accelerate for 100 seconds up to maximum speed, continue at maximum speed and come to a stop, within 15 minutes. A plot of target velocity, actual simulated velocity and the engaged gear is shown in fig. 46. Power produced by the engine and consumed by the wheels and the PTO has been shown on figure 47. Torque and RPM of the engine shaft is shown in fig. 48. Energy production and consumption is shown in figure 49.

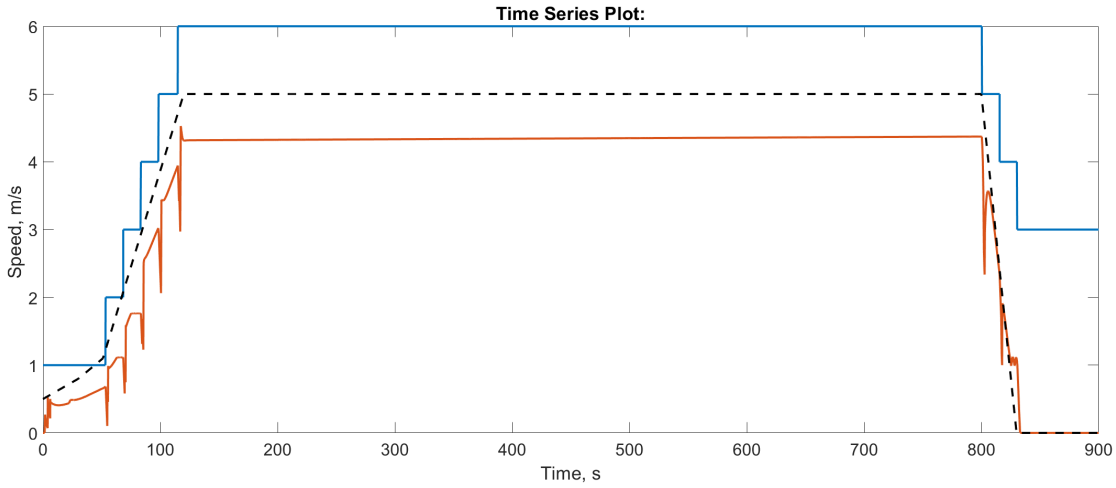

Figure 46: Simulation no.2 velocity and gear plot

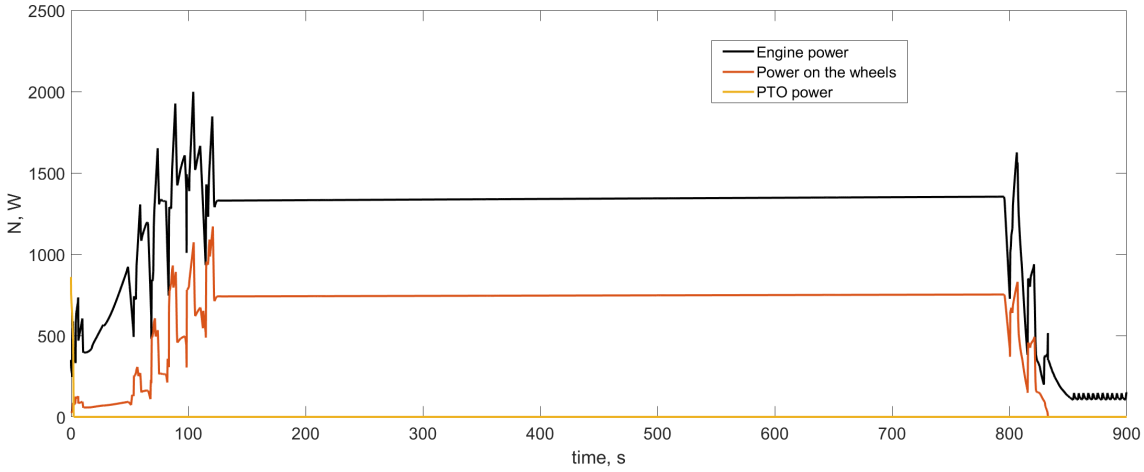

Figure 47: Power plot for simulation no.2, showing power as measured on the engine shaft, wheel axle and the PTO

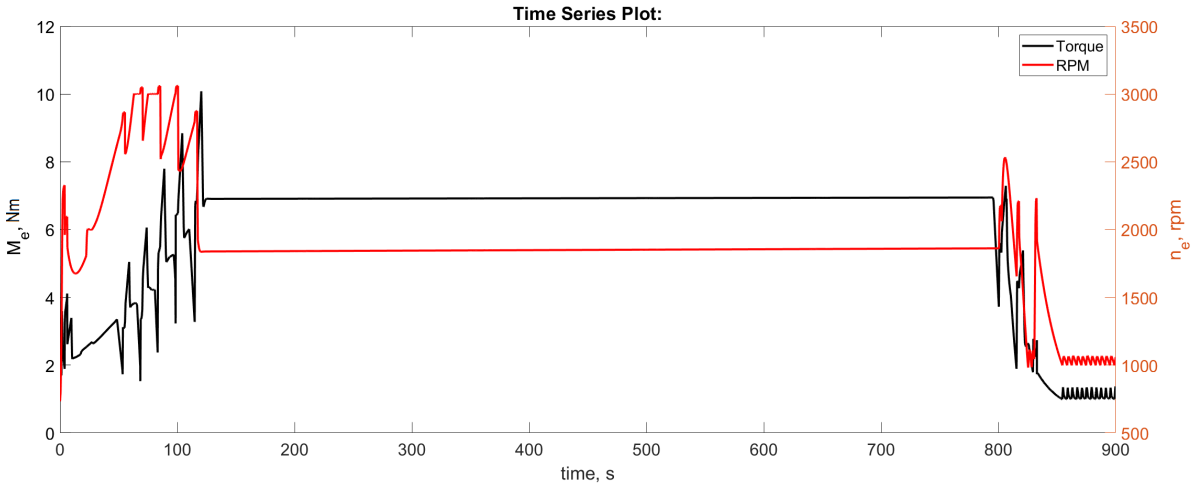

Figure 48: Engine torque and rpm time plots for simulation no.2

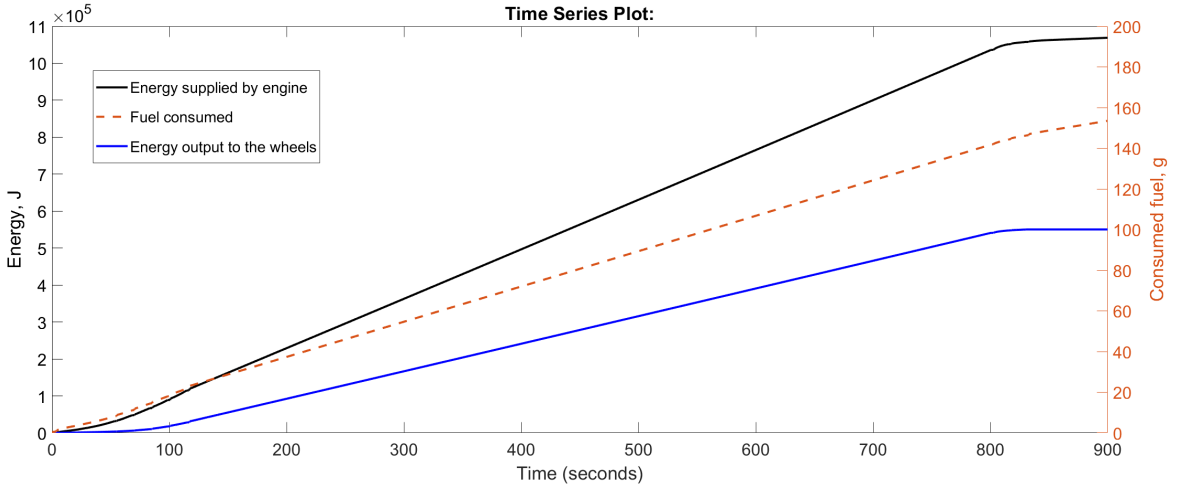

Figure 49: Energy production, consumption and fuel consumption plot for simulation no.2

Overall the distance travelled was 3.21 km and the fuel consumed was 153.48 g.

In another simulation, the tractor is set to quickly accelerate to maximum speed and travel a distance of 100 m. After this, speed is to drop to 1 m/s and this is to continue for another 100 meters. After this the tractor leaves the "field" and can accelerate again, until the overall simulation time reaches a 100 seconds. During the "slow" period the PTO is engaged with the constant friction of 1 Nm. A plot of target velocity, actual simulated velocity and the engaged gear is shown in fig. 50. Power produced by the engine and consumed by the wheels and the PTO has been shown on figure 51. Torque and RPM of the engine shaft is shown in fig. 52. Energy production and consumption is shown in figure 53.

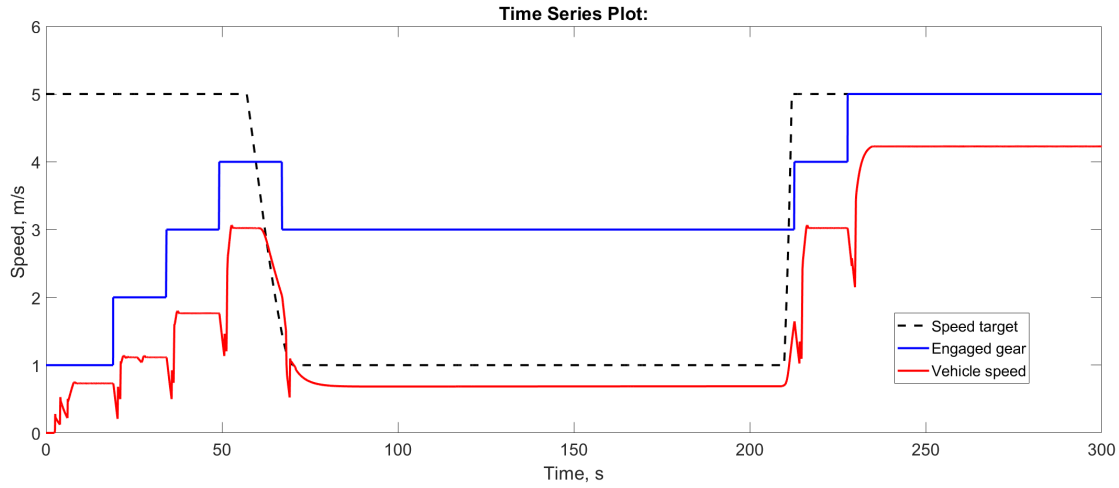

Figure 50: Simulation no.3 velocity and gear plot

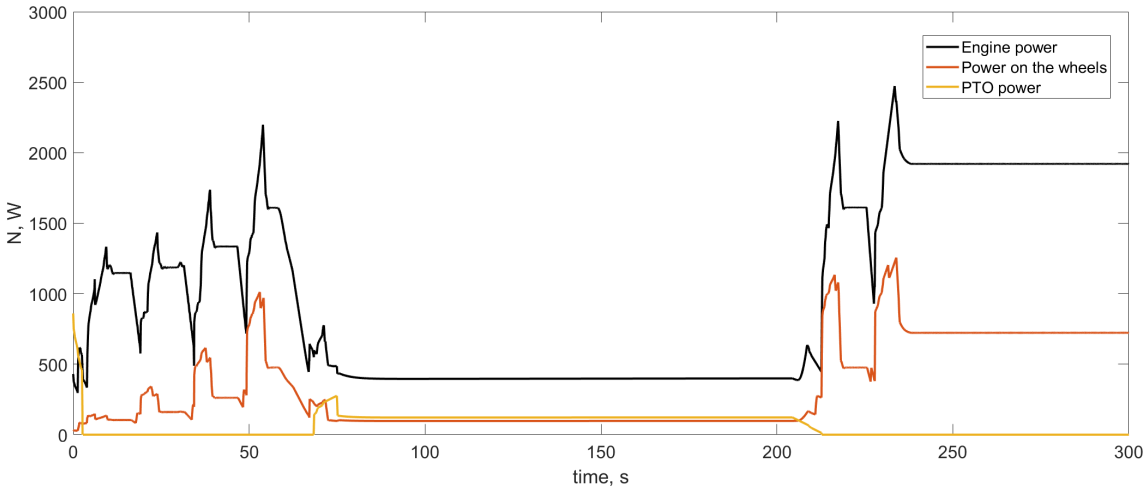

Figure 51: Power plot for simulation no.3, showing power as measured on the engine shaft, wheel axle and the PTO

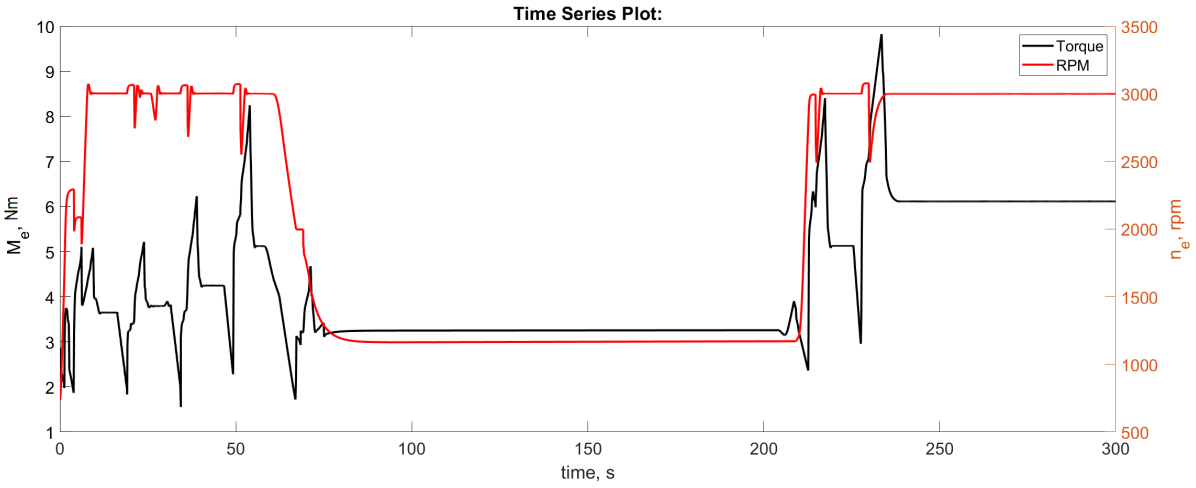

Figure 52: Engine torque and rpm time plots for simulation no.3

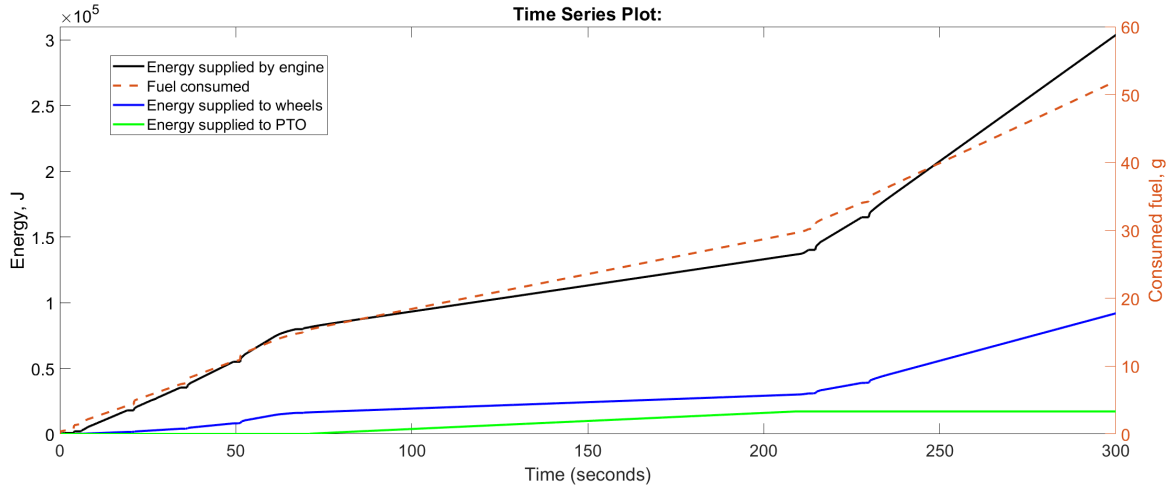

Figure 53: Energy production, consumption and fuel consumption plot for simulation no.3

Overall the distance travelled was 0.543 km and the fuel consumed was 51.95 g.

In another simulation, the tractor is set to quickly accelerate to maximum speed and travel a distance of 100 m. After this, speed is to drop to 1 m/s and this is to continue for another 100 meters. After this the tractor leaves the "field" and can accelerate again, until the same distance is covered as in the previous simulation. During the "slow" period the PTO is engaged with the constant friction of 10 Nm, giving it effectively a power requirement of 1 kW at nominal conditions. A plot of target velocity, actual simulated velocity and the engaged gear is shown in fig. 54. Power produced by the engine and consumed by the wheels and the PTO has been shown on figure 55. Torque and RPM of the engine shaft is shown in fig. 56. Energy production and consumption is shown in figure 57. Overall the distance travelled was 0.543 km and the fuel consumed was 75.29 g.

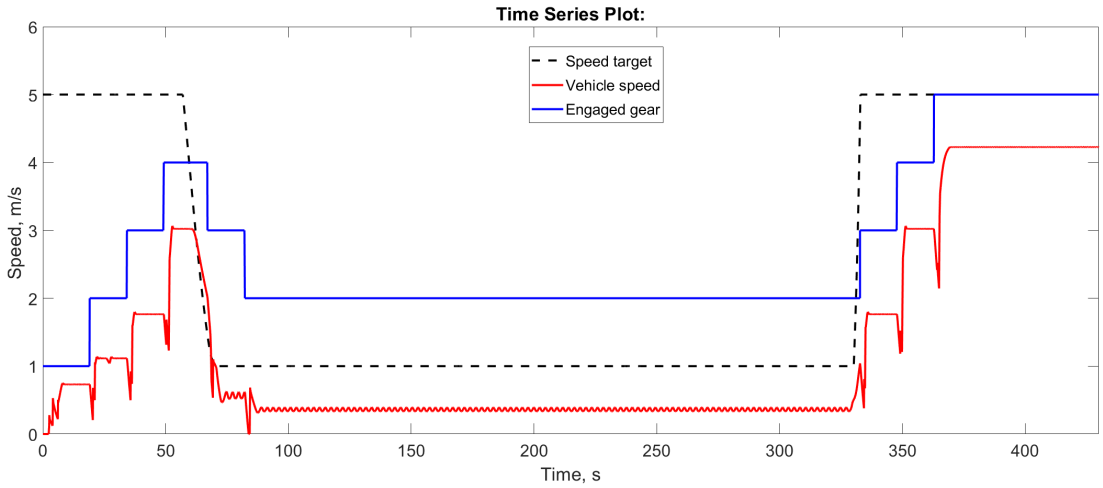

Figure 54: Simulation no.4 velocity and gear plot

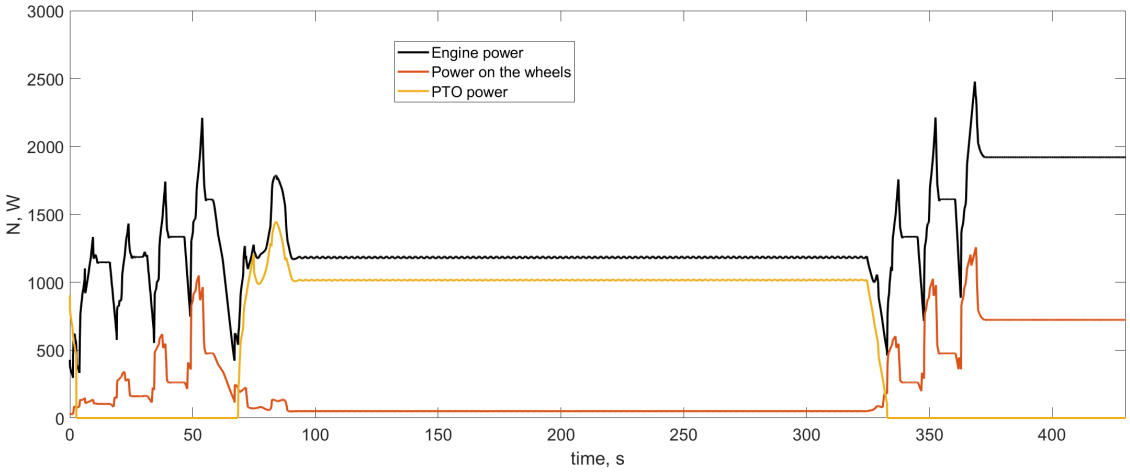

Figure 55: Power plot for simulation no.4, showing power as measured on the engine shaft, wheel axle and the PTO

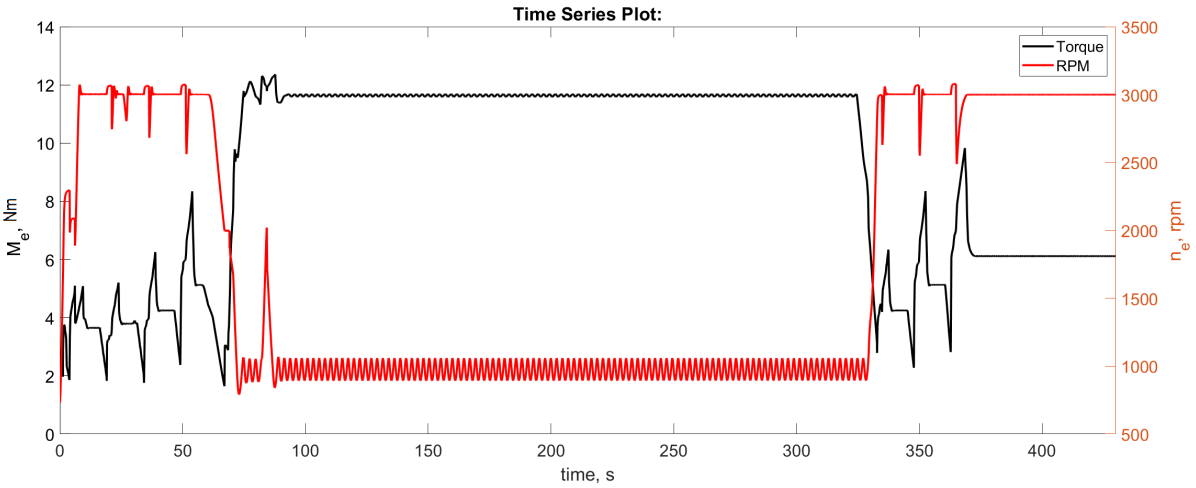

Figure 56: Engine torque and rpm time plots for simulation no.4

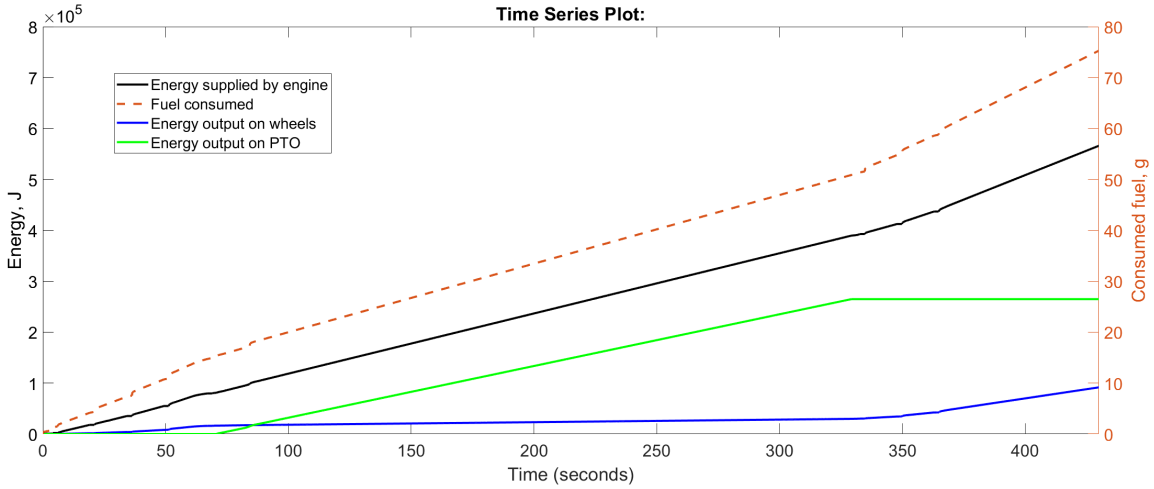

Figure 57: Energy production, consumption and fuel consumption plot for simulation no.4

4 Tractor engine indication tests

The aim of this work was the implementation of a mobile engine indication system into the tractor built for the ACTIVATE project and the carrying out of measurements with this system based on real working conditions. This has been accomplished with the use of the PCA-2000 combustion analysis system. It allows for real time measurement and works in a similar principle. Measurements were carried out on the automotive dynamometer located at the Silesian University of Technology.

The measurements were taken with direct ammonia injection and biodiesel pilot injection, based on an engine map developed with the project.

The measurement system has been utilized previously within the project, however that was within the confines of the stationary engine test rig. The new setup had to be built with available parts and made to work without the angular encoder present in the previous test rig.

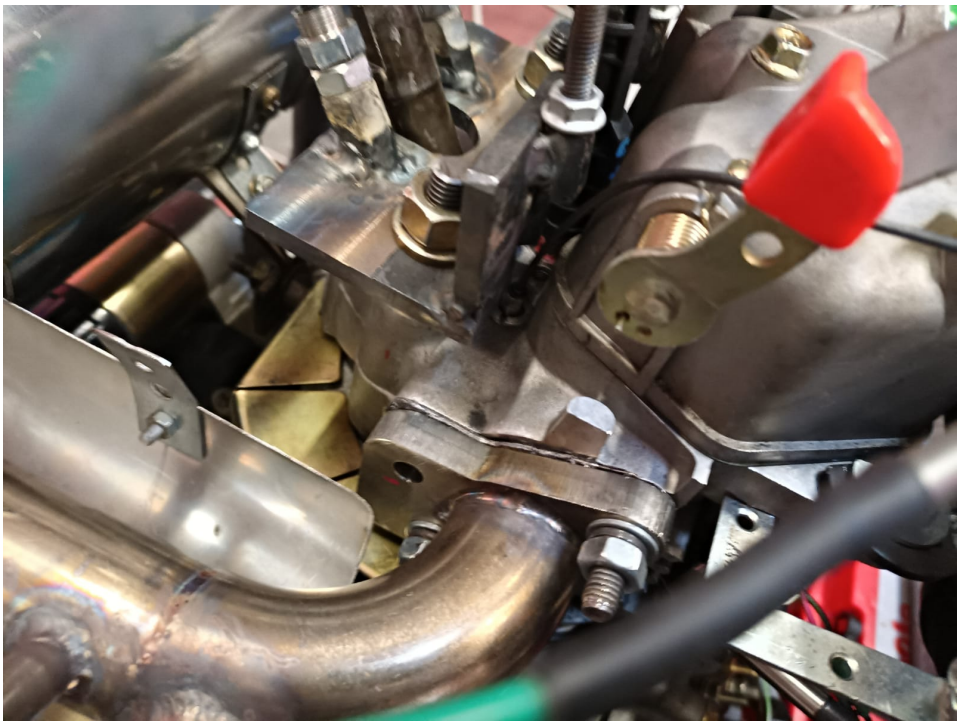

Figure 58: Pressure sensor location on the tractor indication rig.

Measurements were taken with the tractor installed on the chassis dynamometer. The load on the wheels was maintained in the proximity of 60 Nm and the engine speeds were varied between 1800 and 3000 rpm, with an increment of 200. The engine injection control was carried out automatically, by maps created in the course of the project though map adjustments were carried out during these tests. The accelerator pedal had been disconnected and replaced by manual potentiometer so that the engine driver demand did not vary.

Indication results obtained in this session suffered from the problem with signal sampling. The error is visible as a "notch" on the p-V and p-α diagrams in the beginning of the compression phase. This was adjusted for in the subsequent calculations by the creation of a dedicated code in MATLAB, fitting the questionable part of the chart to a line following the equation:

$$pV^{1.33} = \text{idem}, \tag{4}$$

or in other words, to a polytropic compression process. Indicated power has also been calculated using this code instead of the PLEX Combustion Analysis software. The results for each tests were:

1. 1800 rpm - 1.8368 kW,
2. 2000 rpm - 1.9445 kW,
3. 2200 rpm - 2.4223 kW,
4. 2400 rpm - 2.448 kW,
5. 2600 rpm - 2.696 kW,

6. 2800 rpm - 2.857 kW,

7. 3000 rpm - 3.790 kW.

The and p-α charts showing the cycle average, maximum and minimum pressure traces are shown in figures 60 to 66. The p-V charts with raw and corrected pressure traces are shown in the figures below. It should be noted, that the "notch" in the pressure trace is a software error as it is not visible on the oscilloscope signal trace 59.

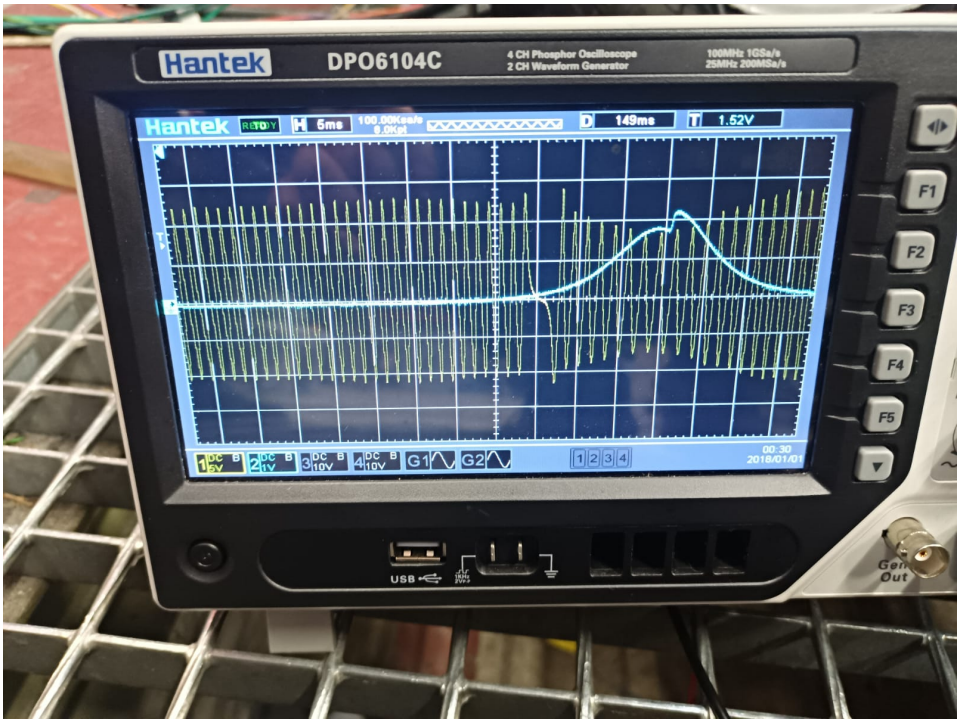

Figure 59: Oscilloscope signal traces; blue - pressure signal, yellow - VR sensor signal.

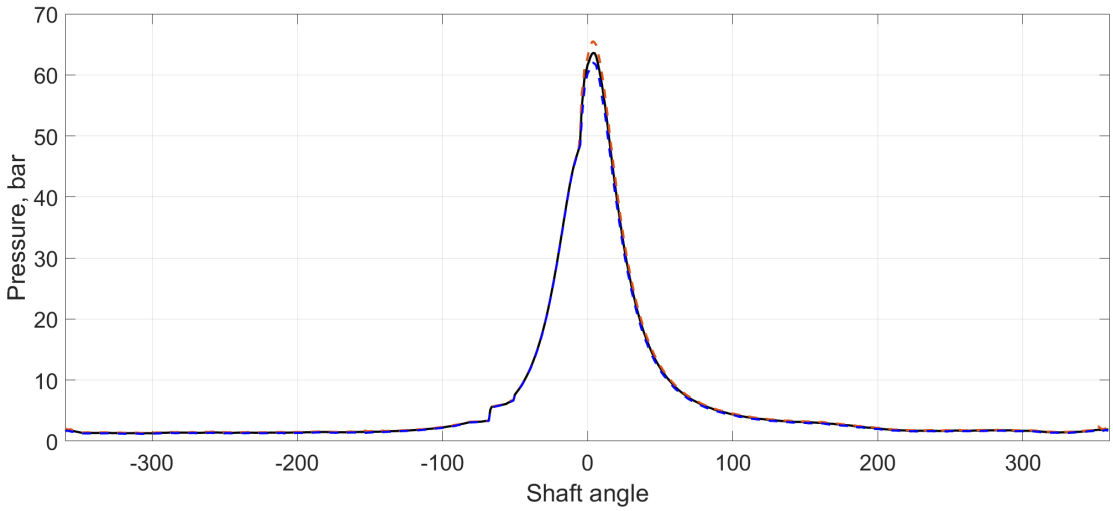

Figure 60: 1800 rpm, angle-pressure chart, showing the cycle average and the maximum and minimum pressure traces.

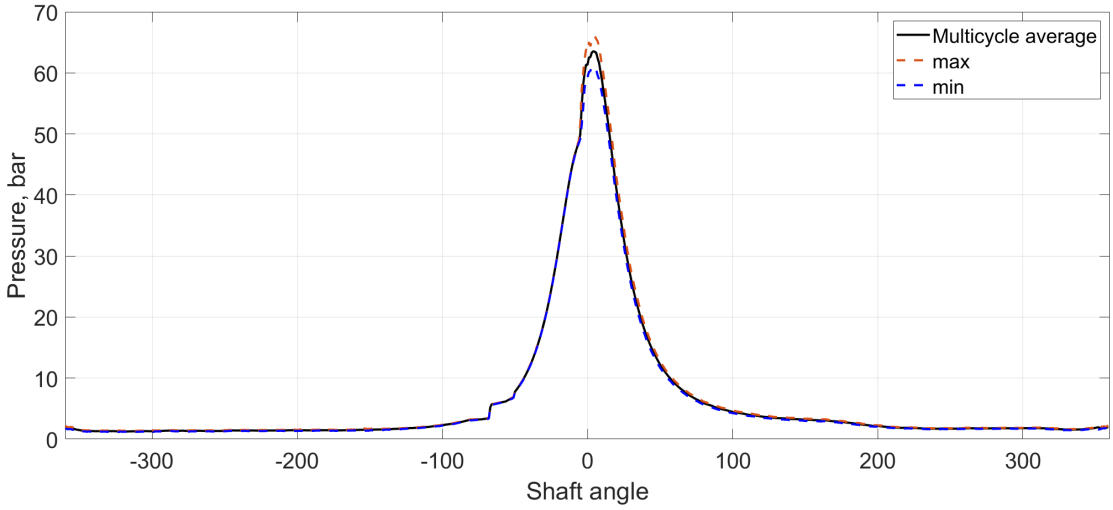

Figure 61: 2000 rpm, angle-pressure chart, showing the cycle average and the maximum and minimum pressure traces.

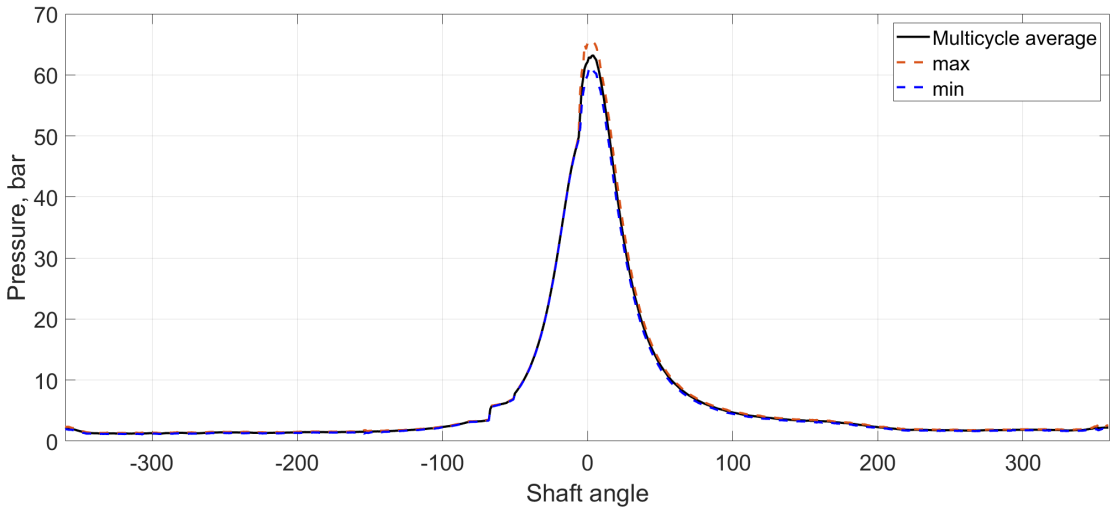

Figure 62: 2200 rpm, angle-pressure chart, showing the cycle average and the maximum and minimum pressure traces.

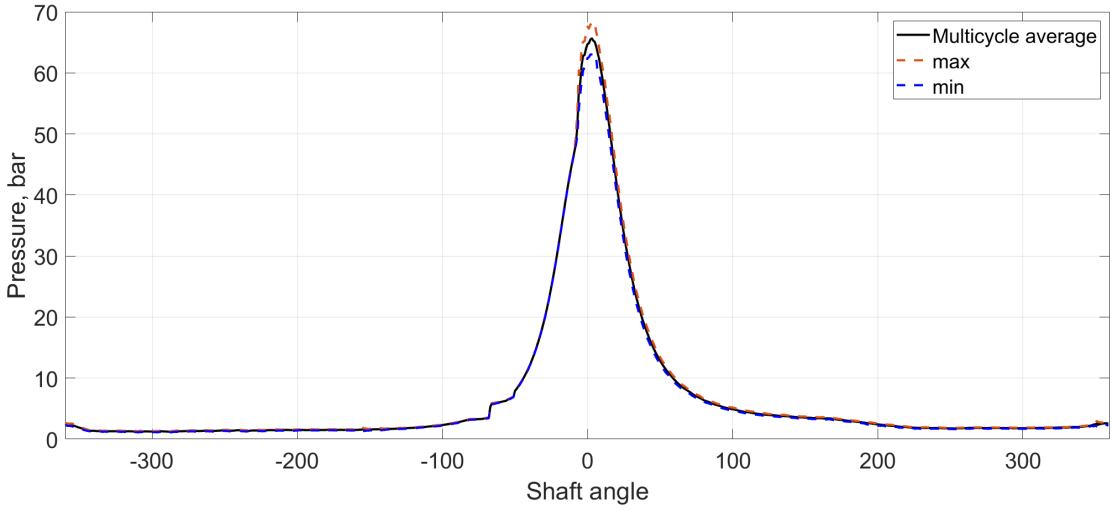

Figure 63: 2400 rpm, angle-pressure chart, showing the cycle average and the maximum and minimum pressure traces.

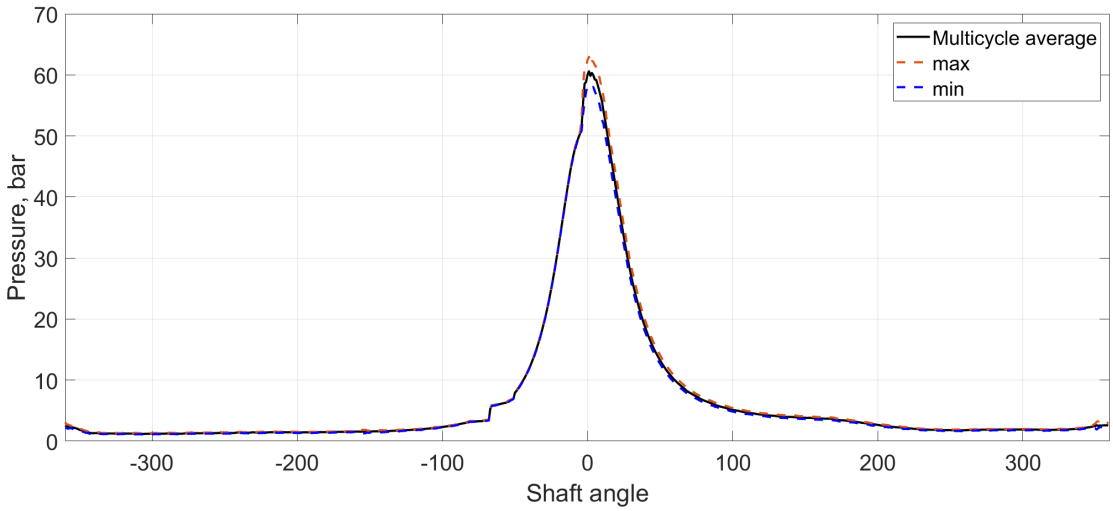

Figure 64: 2600 rpm, angle-pressure chart, showing the cycle average and the maximum and minimum pressure traces.

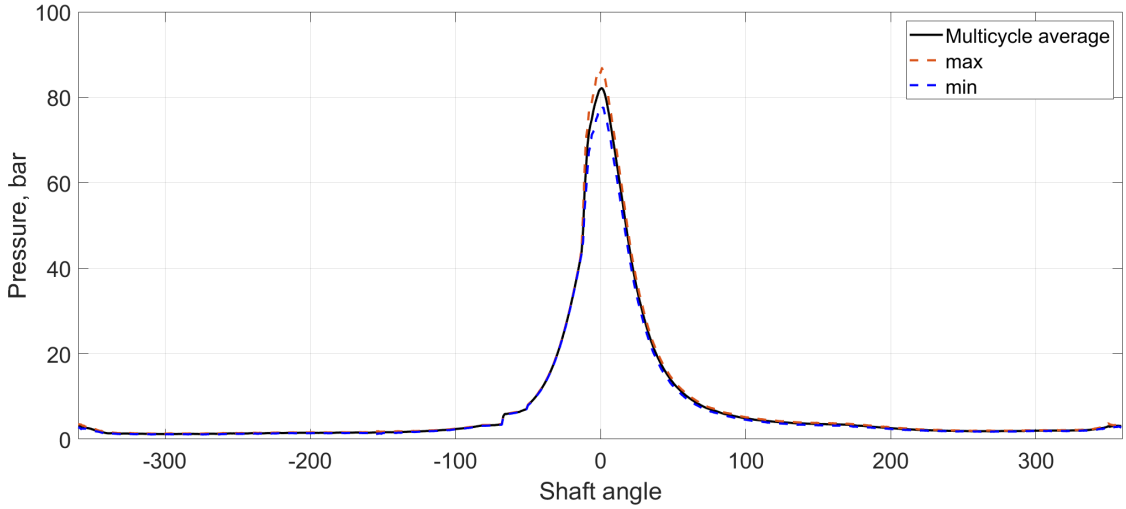

Figure 65: 2800 rpm, angle-pressure chart, showing the cycle average and the maximum and minimum pressure traces.

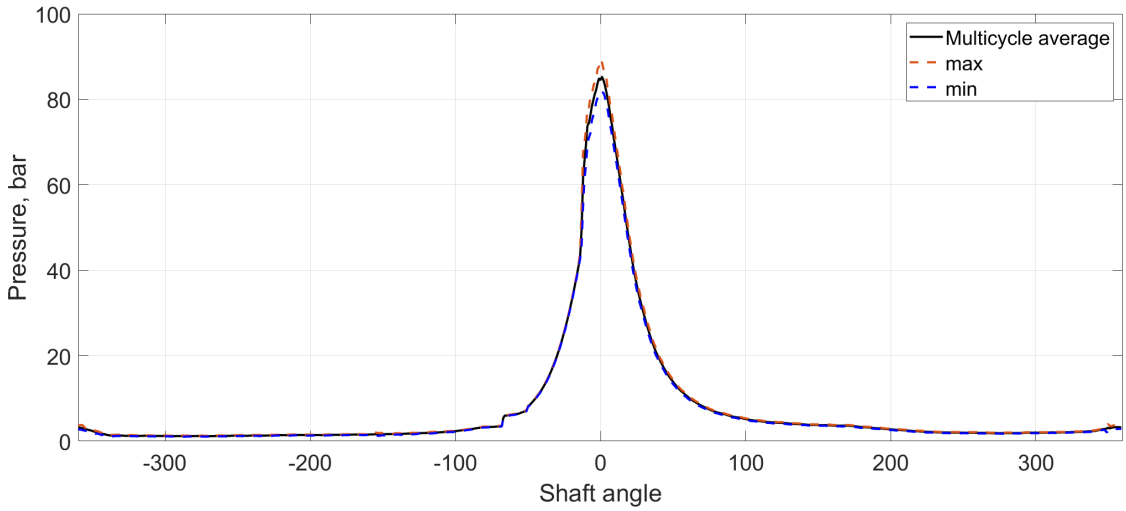

Figure 66: 3000 rpm, angle-pressure chart, showing the cycle average and the maximum and minimum pressure traces.

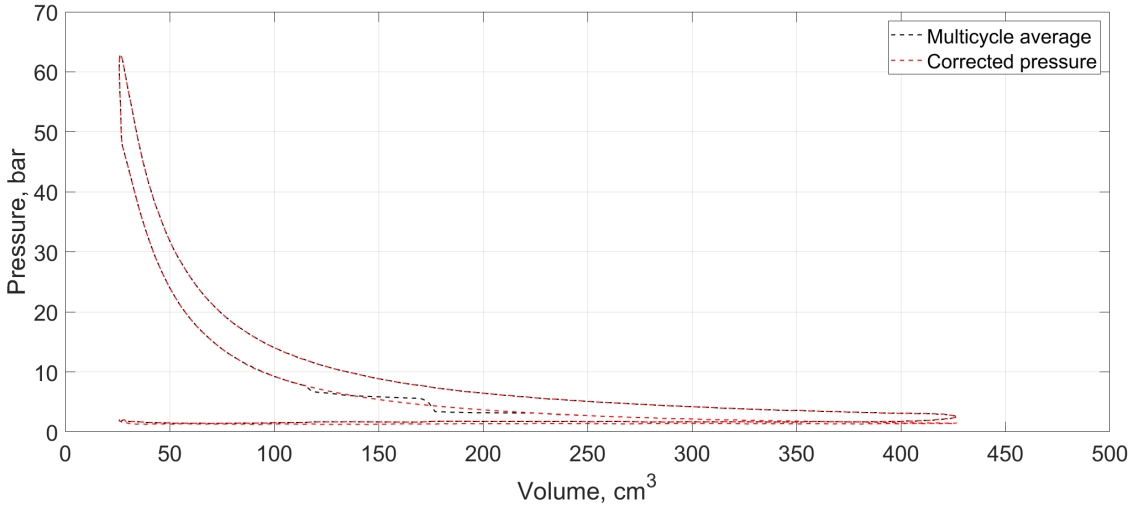

Figure 67: 1800 rpm pressure-volume chart, showing the cycle average raw and corrected (polytropic) pressure trace.

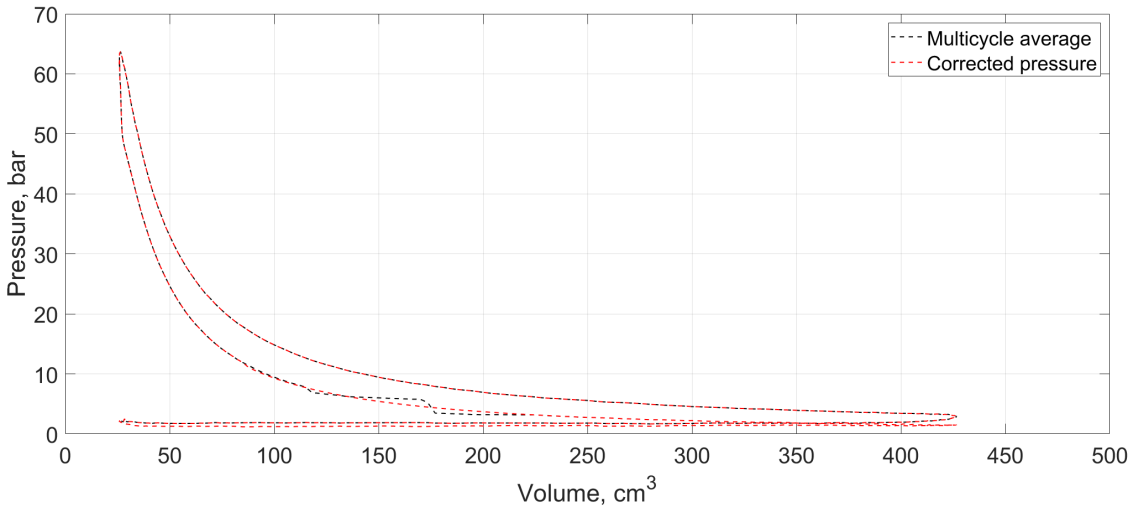

Figure 69: 2200 rpm pressure-volume chart, showing the cycle average raw and corrected (polytropic) pressure trace.

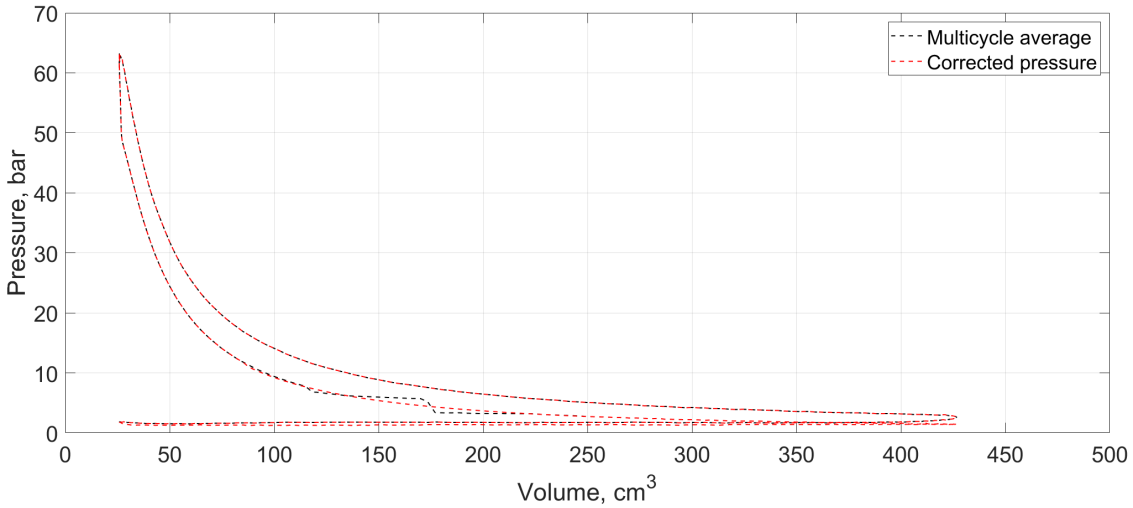

Figure 68: 2000 rpm pressure-volume chart, showing the cycle average raw and corrected (polytropic) pressure trace.

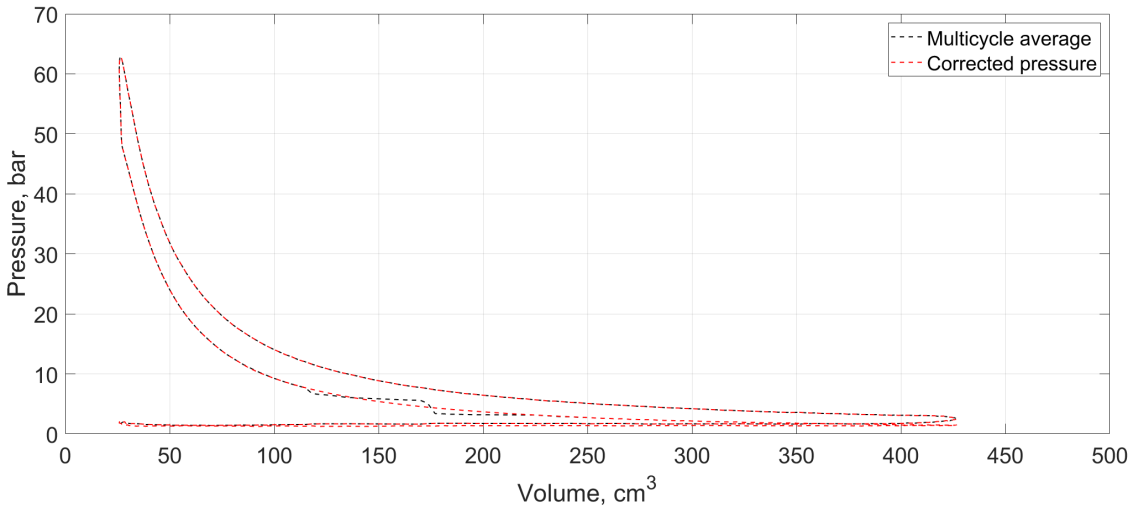

Figure 70: 2400 rpm pressure-volume chart, showing the cycle average raw and corrected (polytropic) pressure trace.

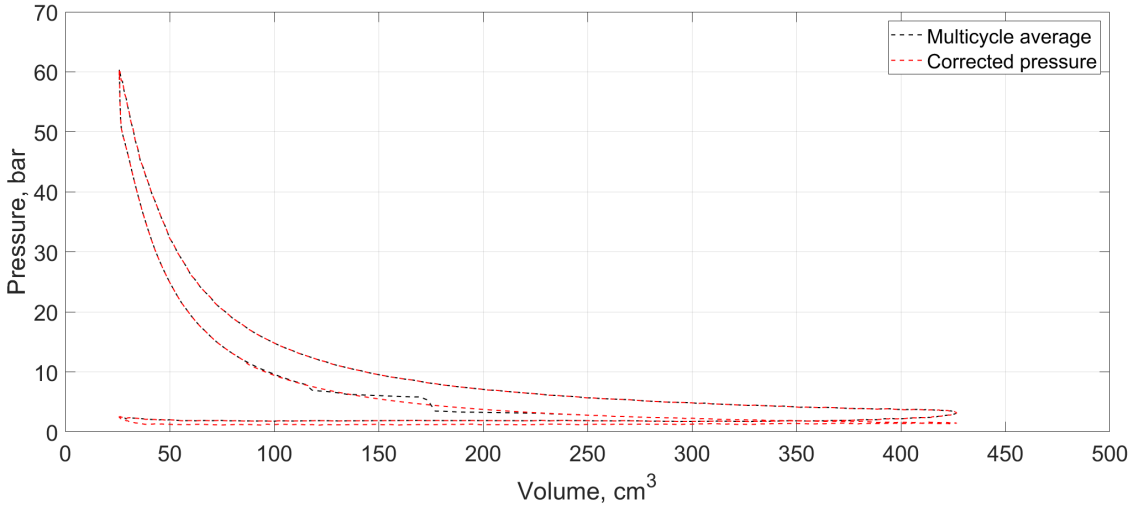

Figure 71: 2600 rpm pressure-volume chart, showing the cycle average raw and corrected (polytropic) pressure trace.

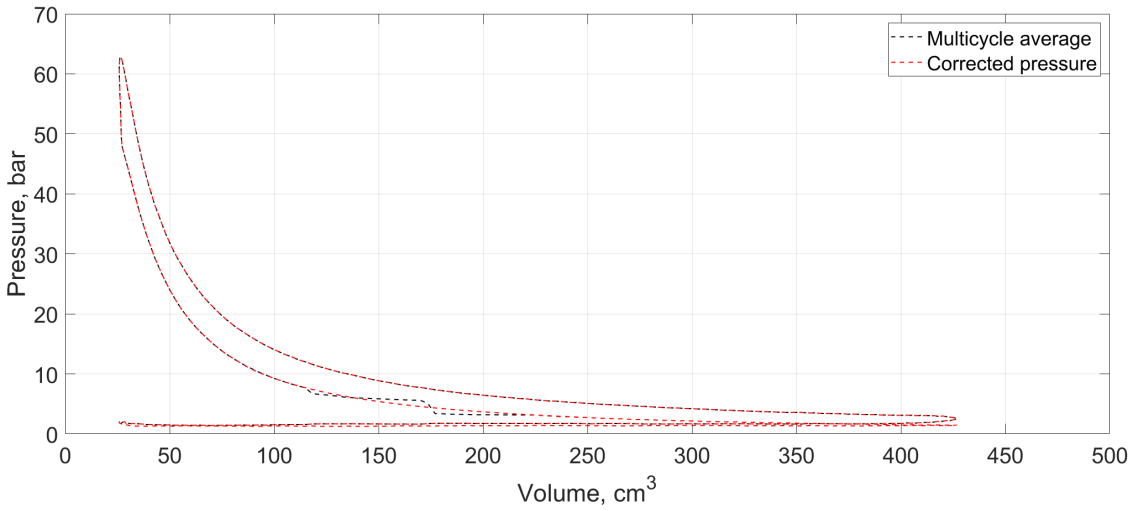

Figure 72: 2800 rpm pressure-volume chart, showing the cycle average raw and corrected (polytropic) pressure trace.

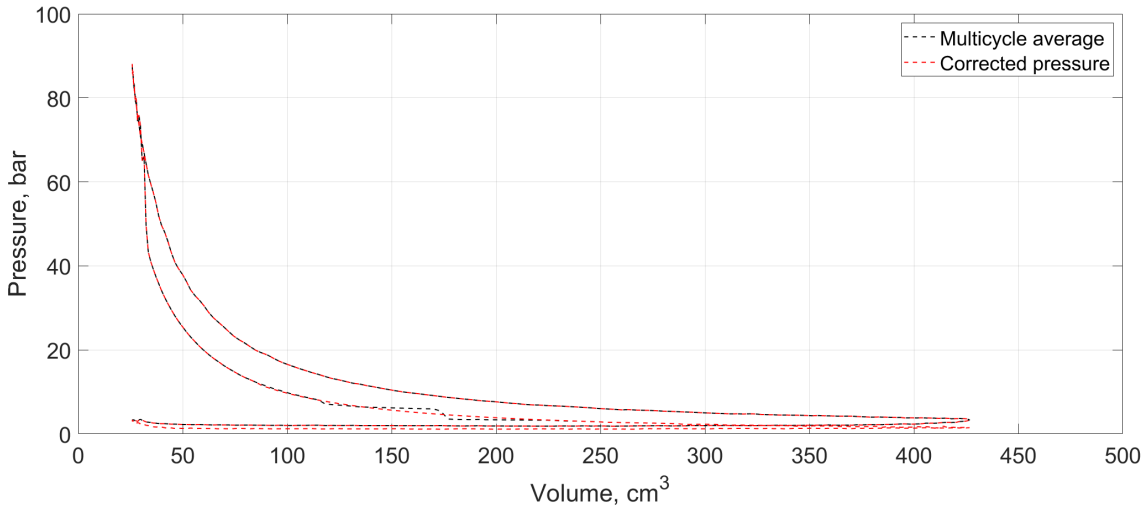

Figure 73: 3000 rpm pressure-volume chart, showing the cycle average raw and corrected (polytropic) pressure trace.

It can be concluded that the PLEX combustion analysis system is adequate for a mobile, vehicular application, however great care needs to be exercised in regards to sensor installation. For future uses, it is recommended that the position sensor be located as close to the BDC as possible if used on a signal wheel connected to a crankshaft. It is however preferable to install it on a camshaft connected wheel, and locate it such, that the marker corresponds to the intake or exhaust phase, due to lesser pressure variations.

From the measurements taken, it should be noted that there is a substantial quantity of mechanical loss in the tractor transmission system. The chassis dynamometer calculated the power on the wheels as in the vicinity of $0..1 - 0.3$ kW - the indicated power was in the range between $1.837 - 3.790$

kW. Though the indicated power can be assumed to have an error due to a possible misreading of the the TDC and likewise erros can exist in the chassis dynamometer reading due to the fact that the tests were carried out in the lower part of the allowable range, this difference is substantial.

5 Publications WP5

5.1 Direct injection strategy of liquid ammonia and biodiesel

The paper entitled **"Experimental and numerical study on direct injection of liquid ammonia and its injection timing in an ammonia-biodiesel dual injection engine"** has been published [1] . In this paper, a CFD study has been carried out to investigate the effects of direct injection of liquid ammonia, ammonia injection strategy and input energy share of ammonia on sprays, mixing process, combustion, ignition, engine performance, and emission characteristics in the dual-fuel ammonia / biodiesel mode. The primary focus of this paper is to explore the possibilities of direct liquid ammonia injection within a dual-fuel mode. It highlights the importance of ammonia's cooling effects and optimizing injection timing to prevent emissions and improve combustion efficiency.

5.2 Injector configurations

The the manuscript titled **"Effects of biodiesel injector configuration and injection timing on the performance, combustion, and emissions characteristics of a liquid ammonia direct injection engine"** has been to the journal for review.

This paper focuses primarily on the configuration of the common-rail (CR) injector, which has been shown to be a key impact on engine performance. By welding three nozzles from the original six-nozzle CR injector, the highest pressure peak and the highest indicated thermal efficiency (ITE) were achieved. This new configuration not only improved the combustion but also substantially reduced the emissions when compared to the original CR injector. The impact of injection timing, another aspect of this paper, was addressed through advancing injecion timing from -24 to -14 CAD, revealing a significant improvement in combustion. The emissions were also analyzed, with the reduction in the number of nozzles in the CR injector leading to a longer injection duration, promoting lean mixture formation during combustion, which significantly reduced CO emissions and resulting in a noticeable reduction in ammonia emissions. Furthermore, this reduction in the number of nozzles significantly reduced NO_x emissions. The influence of injection timing on emissions was also investigated, with an advanced biodiesel injection timing from -24 CAD to -16 CAD yielding an increase in particulate matter (PM) emissions. Furthermore, the study explored specific emissions, including nitrogen oxide (N_2O), carbon dioxide (CO_2), carbon monoxide (CO) and water vapor (H_2O).

5.3 Energy and Exergy analysis

The paper titled **"Energy and Exergy Assessment of Diesel, Biodiesel, and Ammonia Fueled Compression Ignition Engine"** has been published [2], presenting a comprehensive investigation into the performance of a single-cylinder, air-cooled compression ignition engine fueled by diesel, biodiesel, and a biodiesel-ammonia mixture. The study involves a detailed experimental analysis encompassing mass flow rates, temperatures, pressures, and exhaust composition. The research

compares the three fueling strategies and demonstrates that the introduction of ammonia through port injection does not compromise engine performance. Notably, the investigation underscores the promising environmental benefits of using biodiesel-ammonia mixtures, showing potential for reducing greenhouse gas emissions and contributing to decarbonization efforts. The paper's emphasis on exergy analysis also provides valuable insights into optimizing engine performance by addressing exergy destruction associated with combustion and friction processes. The publication serves as a significant contribution to the exploration of alternative fuels for compression ignition engines, paving the way for further research in this critical domain.

References

[1] Ebrahim Nadimi, Grzegorz Przybyła, Terese Løvås, Grzegorz Peczkis, and Wojciech Adamczyk. Experimental and numerical study on direct injection of liquid ammonia and its injection timing in an ammonia-biodiesel dual injection engine. *Energy*, 284:129301, 2023.

[2] Mateusz Proniewicz, Karolina Petela, Andrzej Szlek, Grzegorz Przybyła, Ebrahim Nadimi, Łukasz Ziółkowski, Terese Løvås, Wojciech Adamczyk, et al. Energy and exergy assessments of a diesel-, biodiesel-, and ammonia-fueled compression ignition engine. *International Journal of Energy Research*, 2023.